



Master's thesis

Dark energy parametrization driven bias in cosmological  
parameter estimation

Maria Cavallius

Academic Supervisors:

Steen H. Hansen

Niels Bohr Institute

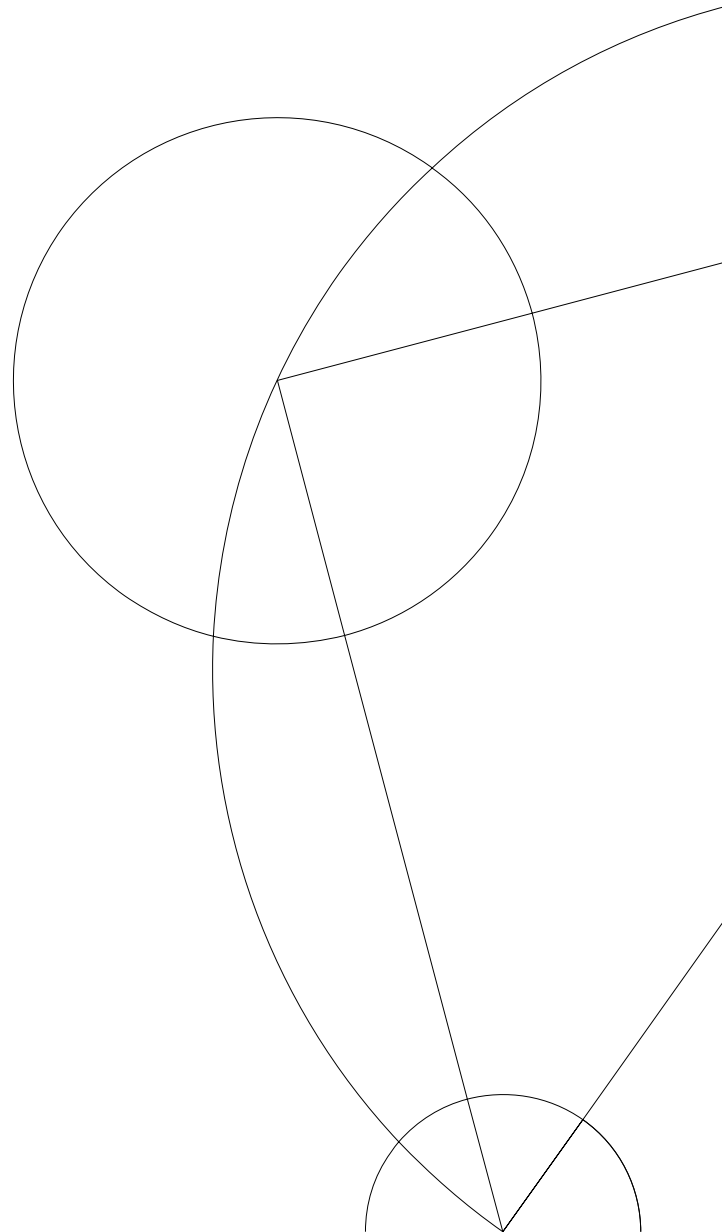
University of Copenhagen

Stefania Pandolfi

Niels Bohr Institute

University of Copenhagen

Submitted: December 22nd, 2014



# Contents

<b>1</b>	<b>Abstract</b>	<b>2</b>
<b>2</b>	<b>Acknowledgements</b>	<b>4</b>
<b>3</b>	<b>The Standard Cosmological Model</b>	<b>5</b>
3.1	Cosmological expansion . . . . .	5
3.2	Two cornerstones of cosmology: isotropy and homogeneity . . . . .	6
3.3	The Friedmann-Lemaître-Robertson-Walker metric . . . . .	7
3.4	The Friedmann equation . . . . .	8
3.5	Energy density components . . . . .	10
3.6	Energy density evolutions . . . . .	12
3.7	The $\Lambda$ CDM universe . . . . .	15
3.7.1	Beyond the Standard Model . . . . .	18
<b>4</b>	<b>Dark Energy</b>	<b>20</b>
4.1	Evidence . . . . .	20
4.2	The cosmological constant and its problems . . . . .	22
4.3	Dark energy alternatives . . . . .	23
4.3.1	The Chevallier-Polarski-Linder model . . . . .	24
4.3.2	The Jassal-Bagla-Padmanabhan model . . . . .	25
<b>5</b>	<b>Observable effects of a redshift dependent equation-of-state</b>	<b>28</b>
5.1	Weak lensing . . . . .	28
5.2	Supernovae Ia . . . . .	32
5.3	Redshift drift . . . . .	35
<b>6</b>	<b>Method</b>	<b>38</b>
6.1	Bayesian inference . . . . .	39
6.2	Monte Carlo Markov Chains . . . . .	40
6.3	Mock data . . . . .	42
<b>7</b>	<b>Results &amp; Discussion</b>	<b>44</b>
7.1	$\Lambda$ CDM fiducial cosmology . . . . .	45
7.1.1	Case 1: weak lensing . . . . .	45
7.1.2	Case 2: supernovae Ia & redshift drift . . . . .	46
7.1.3	Case 3: weak lensing, supernovae Ia & redshift drift . . . . .	47
7.2	JBP fiducial cosmology . . . . .	50
7.2.1	Case 4: supernovae Ia & redshift drift . . . . .	50
7.2.2	Case 5: weak lensing, supernovae Ia & redshift drift . . . . .	51
<b>8</b>	<b>Conclusion</b>	<b>54</b>
<b>A</b>	<b>Appendix</b>	<b>59</b>

# 1 Abstract

The technological advances in observations during recent years have pinned down the values of cosmological parameters to an unprecedented precision. The estimates on the cosmological parameters come from analyses that compare observables to theoretical equations, the form of which is determined by the underlying cosmological model. However, the puzzling dark energy which makes up roughly 70% of the universe's energy density is of a still unknown form. Hence, a crucial yet relatively uncertain part of the cosmological models is the dark energy equation-of-state  $w_{\text{DE}} = P/\rho$ .

This work aims to investigate how a universe governed by one form of  $w_{\text{DE}}$  and analyzed with another gives rise to errors in the cosmological parameter estimates.

Data sets of weak lensing, supernovae type Ia and redshift drift are simulated for both a cosmological constant ( $w_{\text{DE}} = -1$ ) and the scale factor-dependent Jassal-Bagla-Padmanabhan dark energy model ( $w_{\text{DE}}(a) = w_0 + w_a(a - a^2)$ ). The data are fitted to theoretical equations derived from the Chevallier-Polarski-Linder dark energy model ( $w_{\text{DE}}(a) = w_0 + w_a(1 - a)$ ) using a Monte Carlo Markov Chains method. The recovered cosmological parameter probability distributions are compared to the values used to create the simulated data, and the means are found to be shifted. In particular, the present day matter density parameter,  $\Omega_{\text{m}}$ , has a recovered mean value 1.945 standard deviations away from that of the simulated data, while the rms amplitude of mass fluctuations on the scale of  $8 h^{-1}$  Mpc,  $\sigma_8$ , is shifted by 1.511 standard deviations.

## Resumé

De seneste års teknologiske fremskridt indenfor observationel astronomi har fastlagt værdierne af de kosmologiske parametre til en hidtil uhørt præcision. Estimerne af de kosmologiske parametre kommer fra analyser, som sammenligner observable med teoretiske ligninger, hvor sidstnævnte bestemmes af den bagvedliggende kosmologiske model. Formen af den mystiske mørke energi, som udgør ca. 70% af universets energitæthed, er dog stadig ukendt. Dermed er en afgørende, men samtidigt relativt usikker, del af de kosmologiske modeller tilstandsligningen for mørk energi  $w_{\text{DE}} = P/\rho$ .

Hensigten med dette værk er at undersøge, hvorledes et univers styret af én form af  $w_{\text{DE}}$  og analyseret med en anden kan give anledning til fejl i estimerne af de kosmologiske parametre.

Der simuleres datasæt af svag gravitationel lensing, type Ia supernovaer og tidlig ændring

i rødforskydning for både en kosmologisk konstant ( $w_{\text{DE}} = -1$ ) og den skalafaktorafhængige Jassal-Bagla-Padmanabhan model for mørk energi ( $w_{\text{DE}}(a) = w_0 + w_a(a - a^2)$ ). Dataene fittes til teoretiske ligninger udledt fra Chevallier-Polarski-Linder modellen for mørk energi ( $w_{\text{DE}}(a) = w_0 + w_a(1 - a)$ ) ved hjælp af en Monte Carlo Markov Chains metode. De fundne sandsynlighedsfordelinger for de kosmologiske parametre sammenlignes med værdierne brugt til at skabe de simulerede data, og middelværdierne findes at være forskudte. I særdeleshed har tæthedsparameteren for stof i dag,  $\Omega_m$ , en middelværdi 1,945 standardafvigelser fra de simulerede data, mens det kvadratiske gennemsnit af amplituden af massefluktuationer på længdeskalaen  $8 h^{-1}$  Mpc,  $\sigma_8$ , er forskudt 1,511 standardafvigelser.

## 2 Acknowledgements

This thesis is written as part of a master's degree in physics with specialization in astrophysics at the Niels Bohr Institute, University of Copenhagen.

This work would not have been possible without help. Stefania Pandolfi has aided my understanding, guided me along and patiently answered my thousands of questions. As she once told me; “Maria, now is *your* time to be annoying”. I hope I took just enough advantage of that. Steen Hansen has shared his knowledge and experiences, and has always had time for listening to my concerns or ideas. I am deeply grateful to them on both a professional and a personal level.

I owe special thanks to Matteo Martinelli for exchange of ideas and help with programming, without which I would not be very far.

Most of all, I wish to thank my wonderful family and friends. You have encouraged and supported me throughout my education, and I hope you realize how lucky I feel to have you in my life. Thank you Mom, Dad, Jacob and Ruth for always offering me a safe haven in troublesome times. Thank you Linda and Marie for always listening and giving so much of yourselves. Thank you Amanda, Mathilde and Louise for being the best thing I take with me from my university years. And thank you Emil, for you and your love. And for doing all the cooking and cleaning for the last month.

Let's begin.

### 3 The Standard Cosmological Model

The following section is dedicated to introducing cosmological terms and equations. It will become apparent that many of these depend more or less directly on the universe's energy density components and their equations-of-state.

Over the past 25 years or so, technical advances in observations have led to the era of precision cosmology. The new observations have allowed cosmologists to form a coherent picture of the universe and its contents, called the *Standard (Cosmological) Model*.

The theoretical starting point of the Standard Model is general relativity and a specific choice of space-time metric (Dodelson, 2003). This does not by itself explain every observation. However, together with such additions as inflation to explain large scale isotropy and perturbation theory to model structure formation, the Standard Model is able to make quantitative, testable predictions. The predictions are statistical in nature and depend on fundamental physics, and have turned out to stand the test of ever more precise observations. The working model of the universe, which incorporates the additional observational evidence, is called the  $\Lambda$ CDM model for reasons which will become clear in the following sections.

#### 3.1 Cosmological expansion

A fundamental observation to the Standard Model is that the universe is expanding. The present day expansion was first described by Hubble (Hubble, 1929), who in 1929 found the now famous linear relation between a galaxy's recession velocity,  $v$ , and its distance to us,  $r$ , called the *Hubble law*:

$$v = H_0 r, \tag{3.1}$$

where  $H_0$  is the present day value of the *Hubble parameter*, also known as the Hubble constant. For observations, it is customary to quote the dimensionless  $h = \frac{H_0}{100} \text{ km}^{-1} \text{ s Mpc}$ .

Strictly speaking, the linear Hubble law only holds at non-relativistic speeds where the *redshift*  $z$  can be accurately expressed as  $z = v/c$ . The redshift is defined as the wavelength shift of spectral features from the emission wavelength  $\lambda_e$  to the observed wavelength  $\lambda_o$ :

$$z \equiv \frac{\lambda_o - \lambda_e}{\lambda_e}. \tag{3.2}$$

The cosmological redshift is not a Doppler shift, but rather a result of the metric expansion of space, which causes an increase in the photon wavelength (Ryden, 2003).

Taking general relativity into account, the Hubble parameter can be more generally expressed as

$$H(t) = \frac{\dot{a}(t)}{a(t)}, \quad (3.3)$$

where  $a$  is the *scale factor* which expresses the expansion, or contraction, of space as a function of time;  $r(t) = a(t)r(t_0)$ . The scale factor today is normalized so that  $a(t = t_0) = 1$ . The evolution of the scale factor is intimately connected to the energy densities of the various components in the universe.

As the scale factor describes expansion, it is connected to redshift:

$$1 + z = \frac{a(t_0)}{a(t_e)} = \frac{1}{a(t_e)}. \quad (3.4)$$

This means that the Hubble parameter, as any other time-dependent parameter, can be expressed either in terms of redshift or scale factor.

The fact that galaxies are moving away from each other leads to the natural assumption that in the distant past, they were much closer together. This in turn implies that the universe has a finite age, and that galaxies were compressed in an infinitely small volume some specific period of time ago. One can estimate this time as  $t_0 = \frac{r}{v} = H_0^{-1} \approx 14.5$  Gyr, known as the Hubble time. However, if forces such as gravity act on the galaxies, their velocity will not be constant, so the Hubble time is not an accurate measure of the age of the universe.

### 3.2 Two cornerstones of cosmology: isotropy and homogeneity

Galaxies are receding from us according to the Hubble law, and a fundamental assumption is that this picture is the same from every location in the universe. This is an expression of the large scale isotropy about every point in space - and thereby homogeneity - of the universe, which is crucial to the Standard Model. In this context, “large scale” means distances larger than a few hundred Mpc. Isotropy implies that the same observational evidence is available from every direction in the universe, while homogeneity means that the universe will look the same from every observer’s location. Together, the two assumptions make up the *Cosmological Principle*: “There is nothing special about our location in the universe” (Ryden, 2003).

The extreme uniformity of the cosmic microwave background (CMB) - a ubiquitous radiation coming to us from all directions in space - down to 1/10,000 of the temperature (Fixsen, 2009) confirms the assumption of isotropic expansion. Large scale galaxy cluster surveys show that homogeneity holds to good approximation, though there are small deviations from it (Scrimgeour et al. [WiggleZ], 2012).

The two assumptions are crucial for describing the universe with the Friedmann-Lemaître-Robertson-Walker metric as will be done in the following section. The results obtained from those assumptions are fairly simple expressions of observables, used to test data against theory. The assumptions hold very well, but it is worth noting that in a completely uniform universe, structure formation is impossible. Tiny density perturbations, as seen for instance in the cosmic microwave background power spectrum of temperature anisotropies, are the seeds of all stars, galaxies and clusters.

### 3.3 The Friedmann-Lemaître-Robertson-Walker metric

In general relativity, the infinitesimal separation  $ds$  between two events in space-time is given by the metric (Carroll, 2004)

$$ds^2 = g_{\mu\nu} dx^\mu dx^\nu,$$

using the summation convention. The metric tensor  $g_{\mu\nu}$  contains all geometric information, while  $dx^\mu$  is an infinitesimal coordinate displacement.

An isotropic and homogeneous universe of one temporal and three spatial dimensions is described, in spherical coordinates, by the metric tensor

$$g_{\mu\nu} = \begin{pmatrix} -c^2 & 0 & 0 & 0 \\ 0 & 1 & 0 & 0 \\ 0 & 0 & S_\kappa^2(r) & 0 \\ 0 & 0 & 0 & S_\kappa(r)^2 \sin^2 \theta \end{pmatrix} \quad (3.5)$$

yielding the metric

$$ds^2 = -c^2 dt^2 + dr^2 + S_\kappa(r)^2 d\Omega^2.$$

The volume element  $d\Omega^2 \equiv d\theta^2 + \sin^2 \theta d\phi^2$ , while the function  $S_\kappa$  describes the spatial curvature and is given by

$$S_\kappa = \begin{cases} R \sin(r/R) & (\kappa = +1) \\ r & (\kappa = 0) \\ R \sinh(r/R) & (\kappa = -1) \end{cases} . \quad (3.6)$$

The curvature constant  $\kappa$  is 0 for flat space, +1 for a positively curved space (closed geometry) and -1 for a negatively curved space (open geometry).  $R$  is the radius of curvature.

If the distances between objects are allowed to expand or contract as a function of time, one arrives at the *Friedmann-Lemaître-Robertson-Walker* (FLRW) metric:

$$ds^2 = -dt^2 + a^2(t) [dr^2 + S_\kappa(r)^2 d\Omega^2] . \quad (3.7)$$

This useful metric describes an isotropic and homogeneous space-time with the possibility for expansion or contraction as described by the scale factor  $a(t)$ . It was derived independently by Friedmann, Lemaître, Robertson and Walker in the 1920s and 1930s (Friedmann (1922), Lemaître (1933), Robertson (1935), Walker (1935)).

In cosmology it is vital to clearly define times and distances. For instance, the previously stated equation for the scale factor,  $r(t) = a(t)r(t_0)$ , is meaningless without agreement about which observer's time is used and when the distance is measured. The FLRW metric comes in handy at this point.

The time variable  $t$  in the FLRW metric is called the *cosmological proper time* or cosmic time. This is the time measured by an observer moving along with the expansion of the universe, who thus sees a uniform expansion around him. The spatial variables  $(r, \theta, \phi)$  are the *comoving coordinates*, which remain fixed for the described observer. The comoving coordinates label objects at rest in the expanding universe reference frame. In flat space, the comoving distance  $r$  is commonly denoted by  $\chi$  and is given by (Frieman et al., 2008)

$$\chi = \int_0^z \frac{1}{H(z')} dz'. \quad (3.8)$$

The scale factor can now be rigorously defined via the *proper distance*  $d_p(t)$

$$d_p(t) = a(t)\chi. \quad (3.9)$$

The proper distance can be thought of as a physical distance, increasing with the universe's expansion. It is thus the distance between two points when the scale factor is kept fixed (Ryden, 2003).

To describe the time it would take a photon to travel from the furthest observable distance to us today, the *conformal time* is used:

$$\eta = \int_0^t \frac{1}{a(t')} dt'. \quad (3.10)$$

The *angular diameter distance* to an object is its physical size divided by its angular size as seen from Earth. Focusing again only on flat space, the angular diameter distance is related to the comoving distance via

$$d_A(z) = \frac{\chi}{1+z}. \quad (3.11)$$

### 3.4 The Friedmann equation

Friedmann has lent his name to more than the FLRW metric in cosmology. In 1922, seven years before Hubble's observations, Friedmann described the expansion or contraction of an isotropic and homogeneous universe mathematically. He started from Einstein's field equations, which

describe how space-time reacts to the presence of mass-energy (Einstein, 1915),

$$R_{\mu\nu} - \frac{1}{2}Rg_{\mu\nu} = \frac{8\pi G}{c^4}T_{\mu\nu} . \quad (3.12)$$

$R_{\mu\nu}$  is the Ricci curvature tensor, which describes how space deviates from being flat, and  $R$  is the Ricci scalar calculated as  $R = g^{\mu\nu}R_{\mu\nu}$  (where the indices of  $g_{\mu\nu}$  have been raised).  $g_{\mu\nu}$  is the metric tensor, which for the four-dimensional homogeneous and isotropic space-time takes the form of eq. (3.5). Both  $R_{\mu\nu}$  and  $R$  are determined by the choice of metric.

$T_{\mu\nu}$  is the stress-energy tensor, describing the energy density, pressure and stress in space-time. As there is negligible shear stress, viscosity and heat conduction in the universe on large scales, the matter and energy can be modelled as a perfect fluid, meaning it can be characterized entirely by its rest frame energy density  $\rho$  and its isotropic pressure  $P$  (Carroll, 2004). In this case  $T_{\mu\nu}$  is

$$T_{\mu\nu} = (\rho + P)U_\mu U_\nu + Pg_{\mu\nu} . \quad (3.13)$$

Here  $U_\mu$  is the four-velocity. The fluid is at rest in comoving coordinates, so the four-velocity is simply

$$U^\mu = (1, 0, 0, 0) .$$

The energy density and pressure can both be specified for each component of the universe ( $\rho_i$ ,  $P_i$ ) or for the universe as a whole ( $\rho$ ,  $P$ ).

Inserting the chosen metric, Ricci tensor, Ricci scalar and stress-energy tensor into the Einstein equations, the  $\mu\nu = 00$  equation yields the *Friedmann equation* (Ryden, 2003)

$$\left(\frac{\dot{a}}{a}\right)^2 = H(t)^2 = \frac{8\pi G}{3} \sum_i \rho_i(t) - \frac{\kappa c^2}{R_0^2 a(t)^2} . \quad (3.14)$$

The sum is over all components of the energy density. These contribute with different weights to the expansion of the universe, as will be shown later. The curvature could be seen as a sort of energy density, but is here written out separately. The Friedmann equation is extremely useful in cosmology, as it ties together the evolution of the scale factor with the energy density components as well as the curvature.

A flat universe ( $\kappa = 0$ ) has a particularly simple form of the Friedmann equation:

$$\frac{\dot{a}^2}{a^2} = \frac{8\pi G}{3} \sum_i \rho_i(t) . \quad (3.15)$$

The dividing line between positively and negatively curved universes at any time  $t$  is thus given by the *critical density*

$$\rho_c(t) \equiv \frac{3}{8\pi G} H(t)^2 . \quad (3.16)$$

If the total energy density is greater than  $\rho_c$ , the universe must be positively curved, while

a lower value than  $\rho_c$  gives a negatively curved universe. Measurements of the temperature fluctuations of the CMB (Hinshaw et al. [WMAP], 2013; Ade et al. [Planck Collaboration], 2013) reveal that the universe is - at least extremely close to - flat. Hence the critical density can be evaluated as the mean density today, replacing  $H(t)$  for  $H_0$ , giving  $\rho_0 \sim \mathcal{O}(10^{-29} \text{g cm}^{-3})$ .

Rather than the absolute energy density  $\rho$  the dimensionless *density parameter* is often used

$$\Omega(t) \equiv \frac{\rho(t)}{\rho_c(t)} . \quad (3.17)$$

Again, this can be specified for any component ( $\Omega_i$ ) or the universe as a whole ( $\Omega$ ).

If no specific time has been given, it is assumed that present day values are being used. When referring to e.g. the present day matter energy density being approximately 30%, the mathematical formulation is thus  $\Omega_m = 0.30$ .

To add to the confusion, observational cosmologists often use the physical energy density  $\Omega h^2$ . Comparing eq. (3.16) and eq. (3.17) and remembering that  $H(t = t_0) = h \times 100 \text{ km s}^{-1} \text{ Mpc}^{-1}$ , it is clear that  $\Omega h^2$  is equal to  $\rho$  up to a constant.

To sum up the different measures of geometry,

$$\begin{array}{llll} \kappa = -1 & \rho < \rho_c & \Omega_{\text{tot}} < 1 & \text{open/negatively curved} \\ \kappa = 0 & \rho = \rho_c & \Omega_{\text{tot}} = 1 & \text{flat} \\ \kappa = +1 & \rho > \rho_c & \Omega_{\text{tot}} > 1 & \text{closed/positively curved} . \end{array}$$

The  $\mu\nu \neq 00$  parts of the Einstein equations give the *acceleration equation* (Ryden, 2003)

$$\frac{\ddot{a}}{a} = -\frac{4\pi G}{3} \left( \rho + \frac{3P}{c^2} \right) . \quad (3.18)$$

This equation tells us how the expansion of the universe speeds up or slows down with time. A positive pressure represents contraction or slowing down of the expansion.

The last term,  $\rho + \frac{3P}{c^2}$ , is essential. The energy density  $\rho$  is positive for all types of components, but the pressure  $P$  may not be. In particular, if the Universe is dominated by a component  $P < -\rho c^2/3$ , the left-hand side of eq. (3.18) will be positive, meaning that the universe is not only expanding, but that the expansion is accelerating.

### 3.5 Energy density components

The behaviour of the energy densities of the different components can be further investigated. Cosmology deals with dilute gases which have a simple equation-of-state:

$$P = w\rho . \quad (3.19)$$

The perfect fluid model of the universe operates with three kinds of fluids: matter, radiation and dark energy.

*Matter* - or dust - is made up of non-relativistic particles and accounts for most gases and dark matter. Its equation-of-state parameter  $w_m$  is roughly the ratio of the root mean square thermal velocity over the speed of light squared (Ryden, 2003), and is thus very small.  $w_m$  is usually set to zero, yielding  $P_m = 0$ . Remember that even a component with zero pressure will slow down the expansion c.f. eq. (3.18); the non-zero energy density means that gravity is at work.

It is customary to split the matter energy density into two parts; (i) ordinary matter  $\Omega_b$ , where the “b” stands for “baryonic”, though the energy density also includes electrons, and (ii) the more exotic dark matter  $\Omega_c$ , where the “c” refers to the dark matter being “cold”, i.e. having small velocity dispersions. The latter is regarded as necessary for structure formation to take place at an early enough time for galaxy clusters to have grown to the sizes observed today. The non-baryonic dark matter interacts only gravitationally, and therefore neither emits nor absorbs electromagnetic radiation. Its existence is deduced from total mass estimates made with e.g. galaxy rotation curves or CMB anisotropy measurements. These suggest the value of  $\Omega_m$  to be about 30%, though the visible matter and gas only makes up around 5%. The remaining approximately 25% are attributed to the dark matter, which is typically found in the form of halos surrounding galaxies and clusters (Lahav and Liddle, 2014; Hinshaw et al. [WMAP], 2013).

*Radiation* is defined as relativistic particles and includes photons and neutrinos. Although they have zero or tiny masses, their momenta exert pressure. This pressure is connected in a simple way to the radiation energy density, which also works to slow the expansion. The equation-of-state for a relativistic gas is

$$P_r = \frac{1}{3}\rho_r . \quad (3.20)$$

A mildly relativistic gas will have  $0 < w < \frac{1}{3}$ .

Results of two independent studies in 1998 of a particular type of supernova quite unexpectedly showed that the universe’s expansion is accelerating (Riess et al. (1998), Perlmutter et al. (1999)). This will be returned to in much greater detail later on.

A positive acceleration is achieved when a component has  $P < -\rho/3$ , or equivalently  $w < -1/3$ . Very little is known about the properties of any such component, which has been named *dark energy*. It violates general relativity’s Strong Energy Condition by making the effective gravitational mass negative. This in turn means that gravity can be repulsive instead of attractive (Carroll, 2004).

The Standard Model treats dark energy as a vacuum energy with  $P_{\text{vac}} = -\rho_{\text{vac}}$ , i.e.  $w = -1$ .

The corresponding energy density is denoted  $\Lambda$ , explaining why the Standard Model is also called the “ $\Lambda$ -cold-dark-matter” or “ $\Lambda$ CDM” Model. The dark energy in this model is named the *cosmological constant*.

The Dominant Energy Condition states that for a perfect fluid,  $\rho \geq |P|$ , i.e. the energy density must be non-negative and equal to or greater than the magnitude of the pressure. If  $w < -1$  this condition is not met, and  $w$  enters the so-called phantom region. This makes it possible - though not necessary - for sources to violate causality (Carroll, 2004). This makes little sense physically, so the prior assumption of  $-1 < w_{\text{DE}} < -1/3$  is often used.

Note that the bordering case of  $P = -\rho$  does *not* violate the Dominant Energy Condition.

### 3.6 Energy density evolutions

The temporal evolution of the energy densities is now considered. It turns out that the energy densities of the components evolve at different rates, leading to the interesting phenomenon of epochs in which the expansion has been dominated by different components. Either the redshift  $z$  or the scale factor  $a$  is used to measure time, since these are more readily compared to observations than cosmic time.

Requiring energy-momentum conservation by setting the covariant derivative of  $T^{\mu\nu}$  to zero and using the form of eq. (3.19) leads to the *fluid equation* (Ryden, 2003)

$$\dot{\rho} + 3\frac{\dot{a}}{a}(\rho + P) = 0 . \quad (3.21)$$

Substituting  $P$  for  $w\rho$  gives

$$-\frac{3(1+w)}{a} = \frac{1}{\dot{a}} \frac{\dot{\rho}}{\rho} \quad (3.22)$$

and integrating with respect to  $a$  yields

$$\rho \propto \exp \left[ \int_1^a -\frac{3(1+w)}{a'} da' \right] . \quad (3.23)$$

The integral is limited by  $a = 1$ , representing the present day. It is apparent that the evolution of the energy densities depend on the equation-of-state  $w$  and hence is different for each component. The evolution of the energy densities of course also determines the evolution of the density parameters  $\Omega_i$ .

Each energy density’s evolution in time can now be calculated. For the well-known matter and radiation, one can start with general physical considerations.

First consider that  $\rho = nE$ , with  $n$  being the number density and  $E$  the mean energy per particle of whichever component under consideration. The small speed of non-relativistic matter

means that almost all the mean energy per matter particle is in the form of rest mass energy, which remains constant. The number density is inversely proportional to the three dimensional volume,  $n \propto a^{-3}$ . Together, this means that  $\rho_m \propto a^{-3}$ .

For radiation, the number density of photons falls as  $a^{-3}$  as for matter. Further, the energy per particle decreases, since  $E_r = hc/\lambda$  and  $\lambda \propto a$ . The light waves are “stretched” as space expands. The total effect is that  $\rho_r \propto a^{-4}$ . It may seem strange to assume the number density of photons constant, since the creation of new photons is quite literally obvious. However, the energy density of the CMB is so much larger than the energy density of photons emitted by stars that the latter is usually neglected.

Notice how both results agree with the proportionality above (eq. (3.23)) for  $w = 0$  and  $w = 1/3$ , respectively.

For dark energy, the physical intuition fails us. In the case of a cosmological constant  $w = -1$ , eq. (3.23) reduces to  $\rho_\Lambda = \text{constant}$ . As the universe expands, energy must be created at exactly the right rate to keep  $\rho_\Lambda$  constant. This sounds strange indeed, and many cosmologist question whether  $\rho_\Lambda$  is in fact constant, or if it may have some redshift dependence  $w(z)$ . The subject of dark energy will be returned to in much greater detail.

The different energy density evolutions leads to different scale factor evolutions. This is a direct reflection of mass-energy being intimately connected with spatial curvature as described by Einstein’s field equations (eq. (3.12)). For simple cases of  $\rho_i$ , the dependence of the scale factor on time can be calculated as shown below.

If  $w$  is constant eq. (3.23) tells us that  $\rho_i \propto a^{-3(1+w_i)}$ , which means that  $\frac{\dot{a}^2}{a^2} \propto a^{-(1+3w)}$ . To go further one can make the educated guess that the scale factor has a power law dependence on time,  $a(t) \propto t^q$ , which with the proper normalisation yields

$$a(t) = \left( \frac{t}{t_0} \right)^{2/(3+3w)} \quad w \text{ constant, } w \neq -1 \quad (3.24)$$

with  $t_0$  being the age of the universe. Because of the denominator in the exponent, the equation holds only for constant  $w \neq -1$ . A universe dominated by matter thus expands with time as  $a(t) \propto t^{2/3}$ , while a radiation-dominated universe expands at a slower rate of  $a(t) \propto t^{1/2}$ . Notice how the exponent is less than unity in both expressions, indicating that  $\ddot{a}$  is negative; both matter and radiation slow down the expansion.

If dark energy is in the form of a cosmological constant with an energy density  $\rho_\Lambda$ , the Friedmann equation for flat space (eq. (3.15)) is

$$\frac{\dot{a}^2}{a^2} = \frac{8\pi G}{3} \rho_\Lambda . \quad (3.25)$$

The solution to the above is  $a(t) = \exp \left[ \left( \frac{8\pi G \rho_\Lambda}{3} \right)^{1/2} (t - t_0) \right]$ . Hence, a universe dominated by a cosmological constant is expanding exponentially.

If  $w$  is not constant, the specific dependence of  $a$  on time is slightly more complicated.

Plugging eq. (3.23) into eq. (3.17) yields an alternative expression of the density parameter:

$$\Omega(t) = \Omega_0 \exp \left[ \int_1^a -\frac{3(1+w)}{a'} da' \right], \quad (3.26)$$

where  $\Omega_0$  contains both the constant of proportionality from eq. (3.23) and  $\rho_c$ . Notice that  $w$  can still be time dependent. Going back to the Friedmann equation for flat space (eq. (3.15)) and evaluating the critical density today as

$$\rho_{c,0} = \frac{3}{8\pi G} H_0^2, \quad (3.27)$$

it is clear that

$$\frac{\dot{a}^2}{a^2} = \frac{H_0^2}{\rho_{c,0}} \sum_i \rho_i(t). \quad (3.28)$$

Pulling the critical density in under the summation and switching from  $\rho_i(t)/\rho_{c,0}$  to the newly found expression for the density parameter yields another useful version of the Friedmann equation:

$$\frac{\dot{a}^2}{a^2} = H(t)^2 = H_0^2 \sum_i \Omega_{i,0} \exp \left[ \int_1^a -\frac{3(1+w_i)}{a'} da' \right]. \quad (3.29)$$

Given specific equations-of-state, constant or time dependent, it is now possible to derive an expression for the expansion of space.

It is useful to define the quantity  $E(t)$

$$E(t) \equiv \frac{\dot{a}}{a} = \frac{H(t)}{H_0} = \sqrt{\sum_i \Omega_{i,0} \exp \left[ \int_1^a -\frac{3(1+w_i)}{a'} da' \right]}, \quad (3.30)$$

which can be related to the comoving distance of eq. (3.8) with the substitution  $a = 1/(1+z)$ :

$$\chi = \int_0^z \frac{1}{H(z')} dz' = \frac{1}{H_0} \int_0^z \frac{1}{E(z')} dz'. \quad (3.31)$$

$E(t)$  thus links the energy densities and equations-of-state to the physical sizes in the universe. The quantity enters into many other cosmological equations, for instance the look-back time (Peebles, 1993)

$$t_L = \frac{1}{H_0} \int \frac{1}{(1+z')E(z')} dz', \quad (3.32)$$

which is the difference between the age of the universe now and at the time photons were emitted from a source. Integrating from  $z = 0$  to  $z = \infty$  yields the total age of the universe.

To sum up:

Matter/dust	$w = 0$	$P = 0$	$\rho \propto a^{-3}$	$a(t) \propto t^{2/3}$
Radiation	$w = \frac{1}{3}$	$P = \frac{1}{3}\rho$	$\rho \propto a^{-4}$	$a(t) \propto t^{1/2}$
Dark energy	$w < -\frac{1}{3}$	$P < -\frac{1}{3}\rho$		
Cosmological constant	$w = -1$	$P = -\rho$	$\rho$ constant	$a(t) \propto \exp^{H_0(t-t_0)}$

On a practical note, it is common to neglect radiation and only focus on matter and dark energy. The present day energy density of CMB photons is of the order  $10^{-5}h^{-2}$  (Hu et al., 2014), which is at least a factor of  $10^4$  smaller than that of matter or dark energy, as will be apparent in the following. Neutrinos contribute with even less than this, so they are not taken into account either. Further, the statement of space being flat is sometimes written as the curvature density parameter being equal to zero;  $\Omega_k = 0$ .

### 3.7 The $\Lambda$ CDM universe

The widely accepted working model of the Universe is the  $\Lambda$ CDM model. Though the present work is based on a non-constant dark energy equation-of-state, it is assumed that the remaining concepts of the  $\Lambda$ CDM model still apply.

A key idea of the model is that the universe began with the expansion of space from a single point, i.e. the *Big Bang*. The expansion has proceeded at different rates, depending on the dominant energy densities as described above. Since random thermal velocities scale as  $a^{-1}$ , the temperature of the universe decreases with expansion;  $T = T_0/a$ . Hence, the early universe was very small and very hot. Besides the empirical Hubble law, the Big Bang theory rests on extremely well-fitting observations of *light element abundances* and the *cosmic microwave background*.

The light elements were formed when the very young universe had expanded and cooled to a few MeV/ $k_B$  (Dodelson, 2003). This is below the binding energies of typical nuclei, so *nucleosynthesis* could occur. The primordial abundances can be calculated from the nuclear cross-sections and checked against observations of relatively unevolved objects. Primordial deuterium measurements give particularly precise results. Further, the predictions of primordial abundances depend on the primordial baryon energy density, which can be scaled to the relevant time using the relation  $\rho_b \propto a^{-3}$ . Hence, measuring the light element abundances leads to the baryon energy density today. This turns out to constitute only about 5% of the critical density, while the total matter energy density is believed to be about 30% from direct measurements. This means that most of the non-relativistic matter in the universe is in the form of dark matter. The same conclusion can be reached from several other observations, e.g. the discrepancy between mass

estimates from galactic rotation curves and those from visible gas and matter at large radii as first described by Zwicky in 1933 (Zwicky, 1933).

The CMB is one of the most powerful sources of observational evidence for the  $\Lambda$ CDM model. Although the CMB comes from a point in time far later than nucleosynthesis, the universe was still so hot and dense that baryons and photons were tightly coupled in the primordial plasma. Baryons were continually ionized by photons, and the free electrons rendered the Universe opaque as the photons Thomson-scattered off them. This meant that thermal equilibrium was achieved, and the photons would have had a black-body spectrum.

Once the universe had expanded sufficiently for its temperature to drop to about 3000 K, protons could combine with electrons to form neutral atoms in the epoch known as *recombination*. This caused the density of free electrons to drop suddenly. Photons were then able to stream freely for the first time, making the universe transparent. This epoch of *photon decoupling* took place at around 380,000 years after the Big Bang. The ubiquitous CMB is precisely these first streaming photons, carrying an imprint of the physical conditions at decoupling. The radiation appears to come from a spherical surface around the observer; the radius of this shell is called the *last scattering surface* (Ryden, 2003).

The CMB black-body spectrum with a peak temperature of 2.73 K fits the predictions of a uniform radiation exquisitely. Hidden in the apparent uniformity are tiny anisotropies corresponding to small perturbations in the primordial plasma. The temperature and polarisation *anisotropy power spectra* therefore hold a vast amount of information (see fig. [3.1]). They are dominated by acoustic peaks; the result of sound waves in the photon-baryon plasma, frozen into the CMB at recombination. ESA's WMAP and Planck satellites (Hinshaw et al. [WMAP], 2013; Ade et al. [Planck Collaboration], 2013) have measured the spectra to an extreme precision and have thereby constrained many cosmological parameters. The characteristic angular size of the temperature fluctuations across the sky is called the *acoustic scale*. It is determined by two things; firstly the comoving size of the sound horizon at the time of last scattering

$$r_S(z_*) \equiv \int_0^{\eta_*} c_S(\eta') d\eta', \quad (3.33)$$

where  $\eta$  is the conformal time of eq. (3.10) and  $c_S$  the sound speed which depends on the photon and baryon densities; and secondly the angular diameter distance of the observed fluctuations,  $d_A(z_*)$ , defined in eq. (3.11). The acoustic scale is then

$$\theta = \frac{r_S}{d_A}. \quad (3.34)$$

The clear peak locations in the power spectrum make it possible to determine  $\theta$  to good accuracy from only the CMB.

The separation between the cold and hot spots of the CMB also suggests that the universe is

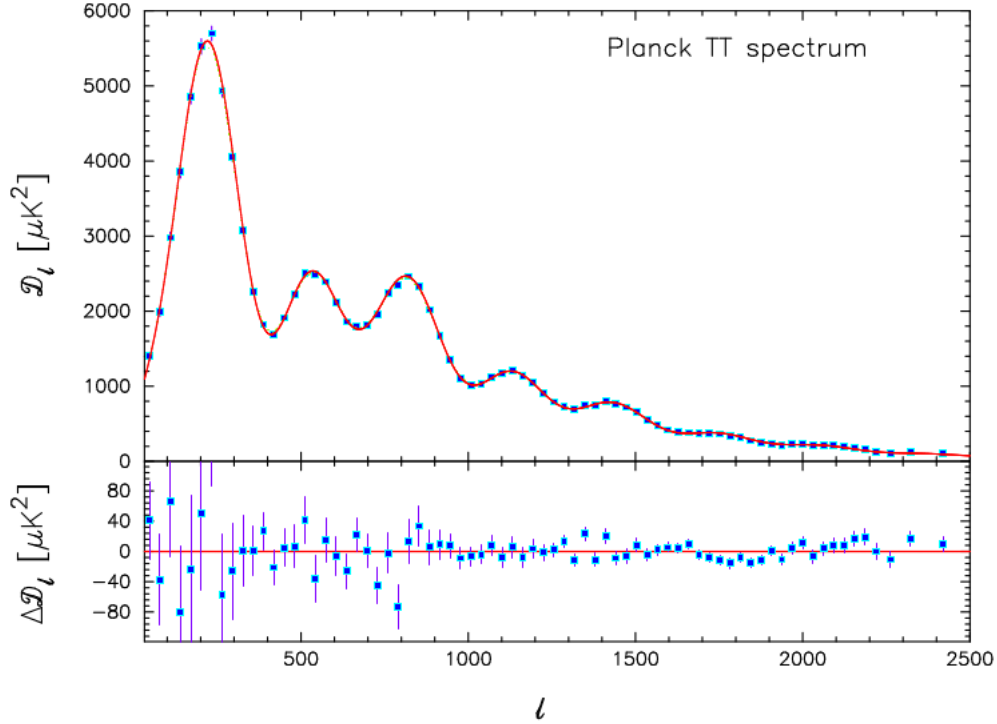


Figure 3.1: The angular power spectrum of temperature anisotropies as measured by the Planck Collaboration. The horizontal axis is multipole moment, which is inversely proportional to angular scale. The vertical axis is  $\mathcal{D}_\ell \equiv \ell(\ell + 1)C_\ell/(2\pi)$ , with  $C_\ell$  being the power spectrum. Points in the upper panel show maximum-likelihood estimates, while the red line is the best-fit  $\Lambda\text{CDM}$  model. The lower panel shows the residuals. Reproduced from (Ade et al. [Planck Collaboration], 2013).

flat (Frieman et al., 2008). In addition to WMAP, other ground-based and balloon-based experiments corroborate the result, though none of these reach WMAP’s margin of error of only 0.4 %. Since the universe is flat, the present day energy density is equal to the critical density, hence the baryonic and dark matter percentages mentioned previously are actually percentages of the present day energy density. Since radiation plays a negligible role, the remaining contribution to the energy density must come from dark energy. This unknown form of energy simultaneously acts as the missing piece in the energy density budget and as the source of the gravitational repulsion causing a late-time acceleration of the expansion.

WMAP and Planck have improved the accuracies of the energy densities by measuring the relative heights of the acoustic peaks in the CMB temperature power spectrum. According to the Planck 2013 best fit results,  $\Omega_\Lambda = 0.68$  and  $\Omega_m = 0.32$  (Ade et al. [Planck Collaboration],

2013). The components of the matter are given as the physical densities,  $\Omega_b h^2 = 0.022$  and  $\Omega_c h^2 = 0.12$ . Interestingly, neither dark matter nor dark energy are predicted theoretically from the Standard Model.

After recombination had taken place and made the universe transparent, there were no other light sources than the cosmic background radiation. This era is therefore known as the Dark Ages. Once the overdense regions that were originally tiny density anisotropies had attracted enough matter for gravitational collapse to occur, structure became more and more pronounced. The first stars, galaxies and quasars were formed, and their radiation ionized the neutral hydrogen. This period, named *reionization*, took place when the universe was  $(0.5 - 1) \times 10^9$  years old. Once the universe as a whole was ionized, radiation was able to escape the quasars and galaxies and travel unimpeded. The optical and infrared light from these first objects is seen at a redshift of about 6 (Dodelson, 2003). At higher redshifts, the neutral medium makes observations increasingly difficult, though the spectra of very luminous quasars can be used. The process is also imprinted in the CMB spectrum as secondary anisotropies, introduced when CMB photons Thomson scatter off electrons during and soon after reionization. The reionization epoch is characterised by the ionization redshift  $z_{\text{re}}$  and the optical depth during reionization  $\tau$ .

### 3.7.1 Beyond the Standard Model

Even with the additions of the Big Bang theory, dark matter and dark energy, observations require further modifications to the Standard Model.

To begin with, our universe has structure on almost every scale. At large scales deviations from homogeneity are small, but present. The small deviations can be included in theories of structure formation through linear perturbation theory, yielding analytical results of the evolution of structure. These can then be held up against observations. Non-linear effects become important at smaller scales where matter has had time to collapse into gravitationally bound structures such as galaxies. The deviations from homogeneity are then too large to be analyzed using perturbation theory. The usual approach to this is N-body simulations of millions or even billions of particles (Dodelson, 2003).

Secondly, there is the question of how the primordial perturbations, which have grown to stars, galaxies and clusters, came to be. *Inflation* answers this in an elegant way. The theory proposes that the universe underwent a phase of exponential expansion at around  $t = 10^{-35}$  sec. Random quantum fluctuations were stretched into small density perturbations, which later acted as seeds of structure formation. After the expansion phase, the potential energy of the field responsible decayed into particles, mainly photons. In this way, the universe was reheated and filled with particles.

Inflation is not yet fully understood, but the simplest models have made predictions that agree

very well with data. The characteristic series of peaks and troughs in the CMB power spectrum is a signature of a simple inflationary model, an adiabatic Gaussian random field of perturbations. The locations and relative heights of the peaks point to a simple form of the *primordial density power spectrum*  $P(k)$  with only two free parameters; the amplitude  $A_S$  and the spectral index  $n_S$ :

$$P(k) = A_S \left( \frac{k}{k_0} \right)^{n_S - 1}, \quad (3.35)$$

where  $k$  is the wave number and  $k_0$  a pivot scale of  $0.05 \text{ Mpc}^{-1}$  (Ade et al. [Planck Collaboration], 2013). The primordial density power spectrum describes the density fluctuations in Fourier space at the end of inflation.

The spectral index measures the deviation from scale-invariance, i.e. the situation in which the amplitude of the primordial perturbations is equal for all scales. Inflationary theory predicts and observations favour a nearly scale-invariant spectrum. Furthermore, inflation would have driven down the value of any primordial curvature energy density, leaving the universe almost flat, as is observed. Also, the fact that the universe is isotropic on scales that would seem to never have been in causal contact acts as evidence for inflation, as they are now allowed to have been close together before inflation began (Frieman et al. (2008), Ryden (2003)).

Inflation further predicts the formation of gravitational waves, which are propagating, transverse perturbations in curvature. The gravitational radiation generates what is known as “B-modes”, or polarization of the CMB. Though the signal is predicted to be extremely small, it was reported detected at the  $7\sigma$  level by the BICEP2 experiment (Ade et al. [BICEP2 Collaboration], 2014). The validity of the results has since been questioned, as the origin of the polarization signal has been proposed to be dust particles in magnetic fields rather than inflation (Adam et al. [Planck Collaboration], 2014). Gravitational waves are tensor perturbations of the curvature, while the temperature perturbations are scalar.

In summary, the universe is almost flat and consists of dark energy, dark matter, baryonic matter and radiation. The dark energy is responsible for an accelerated expansion, not unlike the one that took place during the epoch of inflation, which produced density perturbations from quantum fluctuations. The density perturbations were imprinted in the primordial power spectrum, which takes the form of an adiabatic Gaussian random field and is nearly scale-invariant.

The following section will discuss dark energy, and why it may be a good idea to keep an open mind about its equation-of-state.

## 4 Dark Energy

In 1998, two independent teams studying supernovae type Ia (SNe Ia) found that the universe's expansion is speeding up rather than slowing down, as was expected if only matter and radiation were present (Riess et al. (1998), Perlmutter et al. (1999)).

SNe Ia act as standard candles, meaning they have very uniform peak luminosities and thereby absolute magnitudes. Comparing the observed to the absolute magnitude yields the *luminosity distance*, i.e. the distance the emitted light has travelled. Furthermore, the shift in spectral features of the light curves gives the redshift or, equivalently, the scale factor at the time of emission. The distance-redshift relation can then be mapped, resulting in an expansion history of the universe.

The 1998 discoveries was far from the first time the subject of a repulsive force in the universe was discussed. Einstein had originally added a term  $\Lambda g_{\mu\nu}$  to his field equations to allow for a static, finite universe that would not eventually collapse (Einstein, 1917). As cosmological expansion became the accepted theory, Einstein famously withdrew the  $\Lambda$ , as the Friedmann equation without such a term can model an expanding universe. The cosmological constant has been proposed and withdrawn several times since, but only in 1998 did it become recognized as a part of the consensus model of the universe.

Dark energy affects the expansion rate of the universe, which in turn affects the distance-redshift relation as seen by the two SNe Ia teams. The expansion rate also affects the history of structure formation and thereby the large scale structure observed today (Frieman et al., 2008).

This section will list some of the most convincing pieces of evidence for dark energy, as well as discuss the possible equations-of-state.

### 4.1 Evidence

The controversial conclusion of an accelerating universe in 1998 has since been corroborated by several other observations.

As previously discussed, the characteristic angular size of temperature fluctuations in the CMB suggests that the universe is flat. Independent measurements place  $\Omega_m$  at about 30%, so with negligible radiation about 70% of the energy density is left as dark energy.

A different effect of dark energy is seen at the largest angular scales of the anisotropy spectrum. As photons of the CMB move towards us, they pass through gravitational potential wells of matter. Because of expansion, in part directed by dark energy, the depth of the potential well may change while the photon is in it. The outgoing photon will therefore be either more or

less redshifted than when it entered, depending on whether the potential well has deepened or become shallower. The phenomenon is known as the integrated Sachs-Wolfe effect, and leads to a small correlation between the matter distribution and the CMB anisotropy. Cross-correlating CMB data with galaxy catalogues reveals the effect (Frieman et al., 2008).

Just as the CMB has a characteristic angular scale imprinted in the temperature anisotropy power spectrum, so does the large scale structure have a characteristic length scale imprinted in the matter anisotropy power spectrum. Baryon acoustic oscillations are periodic fluctuations in the density of the baryonic material, caused by sound waves involving baryons and photons in the early universe. After the two components decouple due to expansion, the photons diffuse while the baryons caught in an oscillation stay fixed at the sound horizon at that particular time. Since the baryonic overdensity attracts more matter as time goes on, the characteristic length scale of the sound horizon at decoupling can be used as a standard ruler. This can then be compared to the observed size of matter fluctuations today. A bump is seen in the two-point correlation function of galaxies at about 150 Mpc, which can be held up against theories of structure formation to constrain  $H_0$  (Eisenstein et al., 1998).

The light from galaxies lying behind other gravitational matter is distorted as described by general relativity. The weak lensing technique makes use of this by measuring the statistical signal of shape distortions, yielding among other things an estimate of  $\Omega_m$  and hence also  $\Omega_{DE}$ .

These observational probes are all in excellent agreement with the original results of accelerated expansion and  $\Omega_{DE} \sim 0.7$ .

Explaining the mechanism that generates the acceleration has however turned out to be exceedingly difficult. Either 70% of the universe's energy density is in a completely unknown form with negative pressure, or the laws of general relativity break down on the largest scales.

In the case of dark energy existing as an actual component of the energy density, different approaches are possible. Many different kinds of scalar fields have been proposed to produce dark energy, none of which are without problems of matching the observed energy density to the theoretical. Supersymmetry has also been suggested; if supersymmetry is spontaneously broken at some mass scale, contributions to the vacuum density from fermions and bosons would not cancel each other. However, no supersymmetric particles have yet been discovered experimentally, and the current limits on their mass ranges do not match the dark energy density well. In the active research field of modified gravity cosmic acceleration is seen as a manifestation of unknown gravitational physics rather than a new energy density component. Einstein's equations are edited to produce an effect at large scales which mimics the existence of dark energy.

To compare theory to observations, modified gravity often operates with an effective equation-of-state parameter (Frieman et al., 2008).

Regardless of the mechanism producing the energy, it is possible that  $w_{\text{DE}}$  is either constant or evolving in time. If it is constant, it may take either the form of the cosmological constant  $w_{\Lambda} = -1$ , or any other value consistent with observations. If it is evolving, its dependency on redshift is as of yet unknown to us. Since the equation-of-state plays a part in so many cosmological parameters through the Friedmann equation (eq. (3.29)), it is vital to tackle this topic.

## 4.2 The cosmological constant and its problems

Perhaps the most natural way to explain the unknown energy would be vacuum fluctuations. Even at the lowest energy level, the uncertainty principle dictates that the energy of the universe cannot be exactly zero. Instead, virtual particles are continuously created and destroyed. Such a vacuum energy should take the form of a perfect fluid, hence the stress-energy tensor is again

$$T_{\mu\nu} = (\rho + P)U_{\mu}U_{\nu} + Pg_{\mu\nu} . \quad (4.1)$$

Vacuum energy must maintain Lorentz invariance and be constant in time and space, so the first term involving the four-velocities must be zero. To ensure this,

$$\rho_{\text{vac}} = -P_{\text{vac}} , \quad (4.2)$$

hence,

$$w_{\text{vac}} = -1 . \quad (4.3)$$

Thus vacuum energy is mathematically equivalent to a cosmological constant. The resulting stress-energy tensor is

$$T_{\mu\nu,\text{vac}} = P_{\text{vac}}g_{\mu\nu} = -\rho_{\text{vac}}g_{\mu\nu} . \quad (4.4)$$

The cosmological constant  $\Lambda$  term is to be included in the Einstein field equations (Carroll, 2004)

$$R_{\mu\nu} - \frac{1}{2}Rg_{\mu\nu} + \Lambda g_{\mu\nu} = \frac{8\pi G}{c^4}T_{\mu\nu} , \quad (4.5)$$

Alternatively, one can split the stress-energy tensor into

$$T_{\mu\nu} = T_{\mu\nu,\text{matter}} + T_{\mu\nu,\text{vac}} = T_{\mu\nu,\text{matter}} - \rho_{\text{vac}}g_{\mu\nu} , \quad (4.6)$$

and find

$$R_{\mu\nu} - \frac{1}{2}Rg_{\mu\nu} = \frac{8\pi G}{c^4}(T_{\mu\nu,\text{matter}} - \rho_{\text{vac}}g_{\mu\nu}) . \quad (4.7)$$

Setting the two expressions equal yields a cosmological constant value of  $\Lambda = \frac{8\pi G}{c^4} \rho_{\text{vac}}$ .

Since  $w_\Lambda$  is constant, as the energy densities of radiation and matter go down,  $\rho_\Lambda$  becomes increasingly important. As mentioned, it now constitutes 70% of the total energy density. However, this mathematically simple model raises some important problems that have yet to be solved.

First, there is the *fine-tuning problem*. The energy density of a quantum vacuum is given by

$$\rho_{\text{vac}} = \frac{1}{2} \sum_{\text{fields}} g_i \int_0^\infty \sqrt{k^2 + m^2} \frac{dk}{(2\pi)^3} \simeq \sum_{\text{fields}} \frac{g_i k_{\text{max}}^4}{16\pi^2} \quad (4.8)$$

(Frieman et al., 2008). The sum runs over all quantum fields (e.g. quarks, leptons, gauge fields) and  $g_i$  is the number of degrees of freedom of the field, with a plus for bosons and a minus for fermions.  $m$  is the particle mass and  $k$  the momentum. Since the sum diverges, a cutoff  $k_{\text{max}}$  is required. Quantum field theory is expected to break down at the Planck scale of  $10^{19}$  GeV, and using this as the cutoff gives an energy density of the quantum vacuum that is 120 orders of magnitude larger than the observed value for  $\rho_\Lambda$ . That is spectacularly far off. The fine-tuning needed to obtain the observed value of  $\rho_\Lambda$  causes concerns about the theoretical foundation of the theory.

Secondly, there is the *coincidence problem*. Since  $\rho_\Lambda$  is constant while  $\rho_{\text{matter}} \propto a^{-3}$ , there is only a brief period of time in which the two energy densities are of comparable order. Nevertheless,  $\frac{\Omega_\Lambda}{\Omega_m} = \frac{\rho_\Lambda}{\rho_m} \simeq \frac{0.70}{0.30}$ . It can be argued that this is too unlikely to be true, and that dark energy is probably evolving in time. Others, however, claim that this peculiarity can be solved by the *anthropic principle*: if the value of  $\Lambda$  were not at this perhaps improbable value, it would disturb structure formation, and we would not be around to ask questions about it (Weinberg, 1987).

### 4.3 Dark energy alternatives

If the assumption of  $w_{\text{DE}} = -1$  is abandoned, there are no strong theoretical reasons for believing it to be constant. Different models are then possible, though the new parameters will create new fine-tuning issues. In the so-called quintessence model, the cosmological constant is replaced with a scalar field that allows for an effectively dynamical vacuum energy, meaning that  $w_{\text{DE}}$  can be redshift-dependent (Frieman et al., 2008). The evolving field then accounts for the accelerated expansion of space. This effect can also be reproduced by modified gravity.

It is advantageous to use broad representations of  $w_{\text{DE}}(z)$  rather than one specific model. Using a parametrization of  $w_{\text{DE}}(z)$  allows one to include generic features that are present in different models, and to study the departure from  $w_{\text{DE}} = -1$  in a general way. It is practical to use a small number of parameters to avoid too much fine-tuning.

Common practice in cosmological data analysis is, however, to use either a constant, though not necessarily fixed, value of  $w_{\text{DE}}$  or the simple Chevallier-Polarski-Linder (CPL) parametrization. The final part of this section will be dedicated to introducing the CPL model and another slightly more complex parametrization, the Jassal-Bagla-Padmanabhan (JBP) model. These two models will be the foundation for exploring the effects of different choices of  $w_{\text{DE}}(z)$  on the cosmological parameters.

#### 4.3.1 The Chevallier-Polarski-Linder model

A simple dependence of the dark energy equation-of-state on redshift was discussed by Chevallier and Polarski (Chevallier and Polarski, 2001) and independently by Linder (Linder, 2003). The former considered a toy model with the equation-of-state

$$w(a) = -1 + \alpha + \beta(1 - X), \quad (4.9)$$

where  $X$  is the ratio of the scale factors  $a/a_0$ , and the constants  $\alpha$  and  $\beta$  signify the departure from  $w_0 = -1$  and the amplitude of the time-varying term, respectively. Linder set up the equation slightly differently, choosing not to normalize  $a$ :

$$\begin{aligned} w(a) &= w_0 + w_a(1 - a) \Leftrightarrow \\ w(z) &= w_0 + w_a \frac{z}{1 + z}. \end{aligned} \quad (4.10)$$

The evolution with redshift of the equation-of-state can be seen in fig. [4.1]. Only if  $w_0 \geq -1$  and  $w_a > 0$  does the behaviour remain non-phantom at all times.

The Chevallier-Polarski-Linder, or CPL, model is very widely used, as it has several attractive features. The most obvious is its simplicity teamed with the allowance of a time-varying dark energy density. At low redshift, it reduces to the current value;  $w(z = 0) = w_0$ . The behaviour at high redshift is well-bounded;  $w(z \rightarrow \infty) = w_0 + w_a$ , which isn't true for the linear first-order expansion;  $w(z) = w_0 + w_a z$ . Finally, while the CPL model does not represent any specific theoretical model, the physical interpretation of its two parameters as the present day value and amplitude of the time-varying term, respectively, allows for easy testing of deviations from  $w_{\text{DE}} = -1$ . Note that  $w_a$  is taken as a constant.

The quantity  $E(t) \equiv H(t)/H_0$  is defined in eq. (3.30). Assuming that only matter and dark

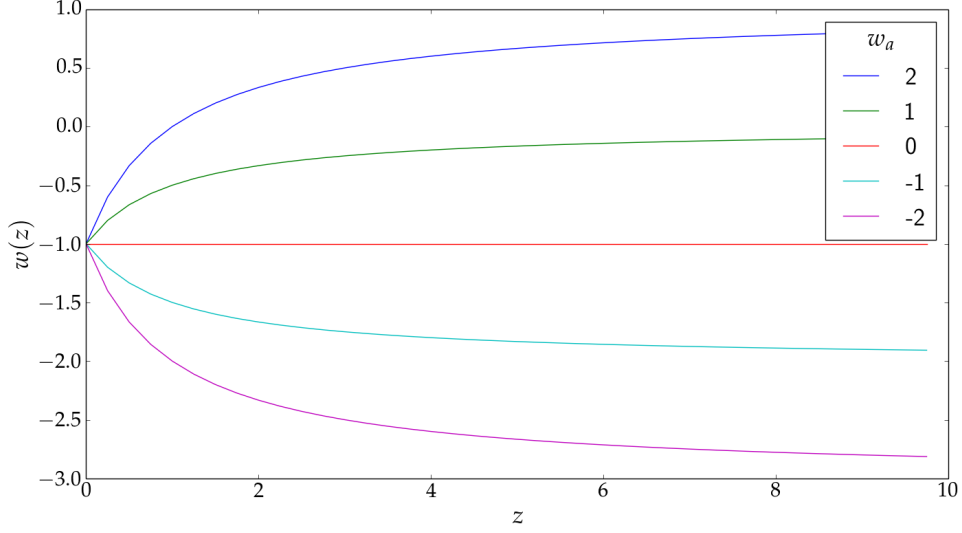


Figure 4.1: Evolution of the dark energy equation-of-state for the CPL model, with  $w_0 = -1$ . Different values of  $w_a$  are shown.

energy contribute to the energy density, and that  $\Omega_{\text{DE}} = 1 - \Omega_{\text{m}}$ :

$$\begin{aligned}
 E(t)_{\text{CPL}} &\equiv \sqrt{\frac{H(t)^2}{H_0^2}} = \sqrt{\sum_i \Omega_{i,0} \exp\left[\int_1^a -\frac{3(1+w_i)}{a'} da'\right]} & (4.11) \\
 &= \sqrt{\Omega_{\text{m}}(1+z)^3 + (1-\Omega_{\text{m}})(1+z)^{3(1+w_0+w_a)} \exp\left[-3w_a \frac{z}{1+z}\right]}.
 \end{aligned}$$

It is clear that the energy density of the dark energy evolves as  $\rho_{\text{DE}} \propto (1+z)^{3(1+w_0+w_a)} \exp\left[-3w_a \frac{z}{1+z}\right]$ . In contrast,  $E(t)$  for the cosmological constant model  $w_{\text{DE}} = -1$  is

$$\begin{aligned}
 E(t)_{\text{CC}} &= \sqrt{\Omega_{\text{m}} a^{-3} + (1-\Omega_{\text{m}})} & (4.12) \\
 &= \sqrt{\Omega_{\text{m}}(1+z)^3 + (1-\Omega_{\text{m}})}.
 \end{aligned}$$

### 4.3.2 The Jassal-Bagla-Padmanabhan model

A slightly different parametrization that also has only two free parameters is the Jassal-Bagla-Padmanabhan or JBP model (Jassal et al., 2005):

$$\begin{aligned}
 w(a) &= w_0 + w_a(a - a^2) \Leftrightarrow & (4.13) \\
 w(z) &= w_0 + w_a \frac{z}{(1+z)^2}.
 \end{aligned}$$

The redshift evolution for a fixed  $w_0 = -1$  is shown in fig. [4.2]. The  $w_0$  parameter is again

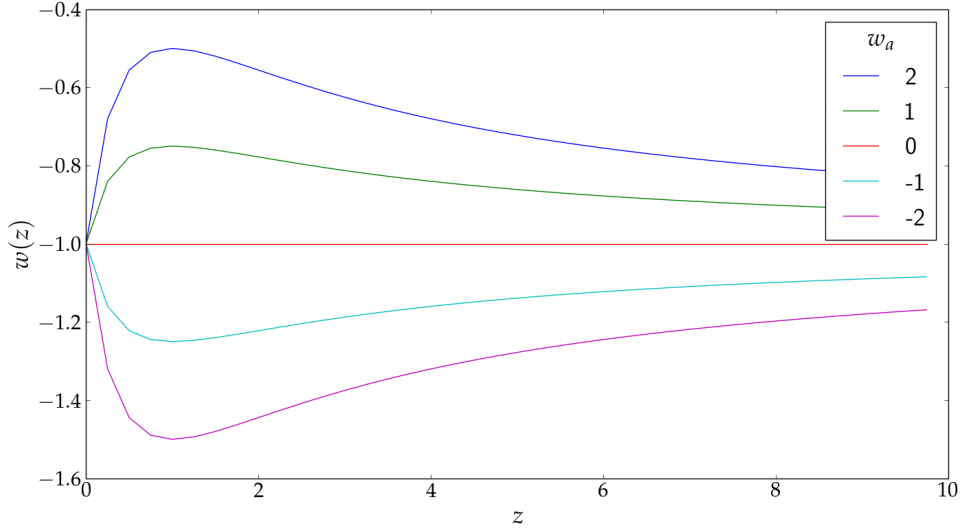


Figure 4.2: Evolution of the dark energy equation-of-state for the JBP model with  $w_0 = -1$ . Different values of  $w_a$  are shown.

the present day value, while  $w_a$  is not directly comparable to that of the CPL model. The JBP model returns to the value  $w_0$  in the distant past,  $w(z \rightarrow \infty = w_0)$ . The model can thus account for theories with  $w_{\text{DE}} \neq -1$  only in a given redshift range, which the CPL model cannot. With regards to ensuring non-phantom behaviour at all times, the JBP model has the same requirements of  $w_0 \geq -1$ ,  $w_a > 0$  as the CPL model does.

The JBP model displays a turning point at  $a = 0.5$  or  $z = 1$  for non-zero  $w_a$ . A further generalization of the model would be to make this turning point redshift-dependent, but this is not in the scope of this work.

As with the CPL model, one can calculate  $E(t)$ :

$$\begin{aligned}
 E(t)_{\text{JBP}} &= \sqrt{\Omega_{\text{m}} a^{-3} + (1 - \Omega_{\text{m}}) \exp \left[ \int_1^a -\frac{3(1 + w_0 + w_a(a' - a'^2))}{a'} da' \right]} \quad (4.14) \\
 &= \sqrt{\Omega_{\text{m}} (1 + z)^3 + (1 - \Omega_{\text{m}}) (1 + z)^{3(1+w_0)} \exp \left[ \frac{3w_a}{2} \left( \frac{z}{1+z} \right)^2 \right]}.
 \end{aligned}$$

Hence, in the JBP model the energy density of dark energy goes as  $\rho_{\text{DE}} \propto (1+z)^{3(1+w_0)} \exp \left[ \frac{3w_a}{2} \left( \frac{z}{1+z} \right)^2 \right]$ .

Though the CPL parametrization is widely used to allow for a more exotic dark energy be-

haviour than a cosmological constant, it may not be the right one. This work aims to demonstrate that forcing one parametrization (e.g. the CPL model) onto a universe governed by a different parametrization (e.g. the JBP model) may cause errors on the cosmological parameter estimates.

With the two chosen models in hand, the next chapter will focus on their effects on observations.

## 5 Observable effects of a redshift dependent equation-of-state

In the previous section, it was argued that there are unresolved problems with the cosmological constant. These problems encourage the exploration of a redshift-dependent dark energy equation-of-state  $w_{\text{DE}}(z)$ . In this section, the effects of such a  $w_{\text{DE}}(z)$  on three different cosmological probes are discussed.

Observable values as a function of redshift, or *mock data*, are produced to mimic different choices of  $w_{\text{DE}}(z)$ . Later sections will study how this ultimately affects the cosmological parameters values.

Since different probes are sensitive to different subsets of cosmological parameters as well as different redshift ranges, three complimentary probes are chosen; weak lensing (WL), supernovae type Ia (SN Ia/SNe Ia) and redshift drift (RD). In particular, redshift drift data spans a redshift region which has traditionally been difficult to probe.

### 5.1 Weak lensing

The light from a distant galaxy may pass through the gravitational potential wells of structure on its way to us. Since mass curves space, the structure acts as a lens, distorting the galaxy's shape. This can result in the galaxy appearing with an elongated shape, and the image can be magnified or even multiplied.

Lensing provides a way of measuring the mass of the intervening matter without any assumptions about its dynamical properties or composition. In particular, lensing does not discriminate between baryonic and dark matter. This can be extremely useful, as dark matter makes up most of the gravitational matter but is difficult to detect directly. Since dark energy influences the distribution of dark matter, mapping the latter via weak lensing can constrain the dark energy equation-of-state.

To relate the observed angular position of the source to its true position, the deflection angle  $\alpha$  is used, see fig. [5.1]. Let  $\theta_S$  be the angular position of a light ray in the source plane, and  $\theta$  the angular position of the same light ray in the lens plane. Defining  $\chi_S$  and  $\chi_{LS}$  to be the comoving distance to the source and between the lens and source, respectively,  $\alpha$  can be obtained via the lens equation (Bartelmann and Schneider, 2001)

$$\alpha = (\theta - \theta_S) \frac{\chi_S}{\chi_{LS}}. \quad (5.1)$$

When  $\alpha$  is small the effect is known as weak lensing, and only one, slightly distorted image is

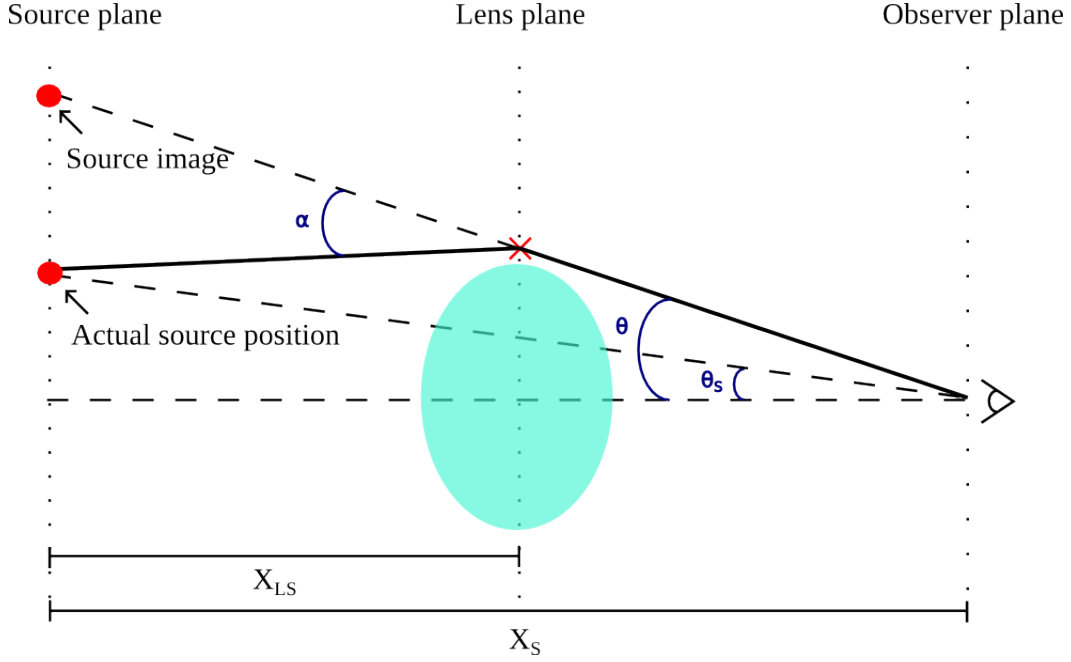


Figure 5.1: Schematic drawing of the bending of light from a source galaxy by an intervening lens. The deflection angle  $\alpha$  between the actual and the observed positions of the source is shown.

seen. This scenario corresponds to the surface density of the intervening matter being much smaller than some critical value (Huterer, 2010). Equation (5.1) then provides a one-to-one and invertible mapping between the source and lens plane positions. In this case the mapping of the galaxy image is described through the distortion tensor

$$A_{ij} \equiv \frac{\partial \theta_S^i}{\partial \theta^j} - \delta_{ij} = \begin{pmatrix} -\kappa - \gamma_1 & -\gamma_2 \\ -\gamma_2 & -\kappa + \gamma_1 \end{pmatrix}, \quad (5.2)$$

where  $\kappa$  is the dimensionless surface mass density or *convergence* of the lens,  $\gamma \equiv \gamma_1 + i\gamma_2$  is the complex *shear* of the observed image and  $\delta$  is the Kronecker delta. The shape distortion is caused by the tidal gravitational field described by shear, while the magnification is a result of both isotropic focusing by  $\kappa$  and anisotropic focusing by  $\gamma$ . In the weak lensing limit,  $|\kappa|, |\gamma| \ll 1$ .

To link  $\kappa$  and  $\gamma$  to cosmological observables, first recall the FLRW metric of eq. (3.7) in flat space with the radial component now denoted by the comoving distance:

$$ds^2 = -dt^2 + a^2(t) [d\chi^2 + \chi^2 d\Omega^2]. \quad (5.3)$$

To describe perturbation of the metric around the lens, Newtonian gauge is used:

$$ds^2 = -(1 + 2\Psi)dt^2 + a^2(t)(1 - 2\Phi) [d\chi^2 + \chi^2 d\Omega^2], \quad (5.4)$$

where  $\Psi$  and  $\Phi$  are the gravitational potentials. If there are no anisotropic stresses, the stress-energy tensor is invariant under spatial rotations, and  $\Psi = \Phi$ .

Shear is defined as

$$\gamma = \gamma_1 + i\gamma_2 = \frac{1}{2} (\psi_{,11} - \psi_{,22}) + i\psi_{,12}, \quad (5.5)$$

where  $\psi_{,ij} = -\frac{1}{2} \int g(\chi) (\Psi_{,ij} + \Phi_{,ij})$ .

$\psi$  is the two-dimensional deflection potential, or projected Newtonian gravitational potential (Bartelmann and Schneider, 2001). The commas denote derivatives with respect to the direction perpendicular to the line of sight. The function  $g(\chi)$  takes the form

$$g(\chi) = \chi \int_{\chi}^{\chi_H} n_{\text{gal}}(\chi') \frac{\chi' - \chi}{\chi'} d\chi' \quad (5.6)$$

where  $\chi_H$  is the comoving distance to the horizon. The number of galaxies per redshift interval per steradian is denoted  $n_{\text{gal}}(z)$ , and  $n_{\text{gal}}(\chi) = H(z)n_{\text{gal}}(z)$ . The quantity is normalized so that  $\int n_{\text{gal}}(\chi) d\chi = 1$ .

Convergence is given by

$$\kappa = \frac{1}{2} (\psi_{,11} + \psi_{,22}). \quad (5.7)$$

Conveniently, the convergence in any direction on the sky  $\hat{\mathbf{n}}$  can be directly related to the distribution of matter. It can be expressed as a weighted projection of the density fluctuation  $\delta(\chi)$  along the line of sight:

$$\kappa(\hat{\mathbf{n}}, \chi) = \int_0^{\chi_h} W(\chi') \delta(\chi', \theta) d\chi' \quad (5.8)$$

where the weighting function is

$$W(\chi) = \frac{3\Omega_m H_0^2}{2a(\chi)} g(\chi). \quad (5.9)$$

Furthermore, photometric redshifts of the sources can be used to map the three-dimensional distribution of matter. The method of dividing the source objects into redshift bins is known as *tomographic* reconstruction of the density field. The convergence and the weighting function are generalized for the  $i$ th redshift bin by the substitutions

$$\kappa(\theta) \rightarrow \kappa_i(\theta) \quad \text{and} \quad W(\chi) \rightarrow W_i(\chi). \quad (5.10)$$

The galaxy distribution of the  $i$ th redshift bin is obtained through the substitution

$$n_{\text{gal}}(z) \rightarrow n_i(z) \quad (5.11)$$

Here  $n_i(z)$  is the number of galaxies per redshift interval per steradian in the  $i$ th bin, and  $\sum_i n_i(z) = n_{\text{gal}}(z)$ . The comoving density of galaxies is  $n_i(\chi) = H(z)n_i(z)$ . If  $\chi'$  in the  $g(\chi)$  integral of eq. (5.6) falls outside the distance range defined by the redshift bin,  $n_i(\chi)$  is zero.

Taking advantage of the relation between convergence and matter density requires a statistical description of weak lensing. While the lensing of individual galaxies by large scale structure cannot be predicted theoretically, the statistical correlations of convergence can, and the prediction is cosmology-dependent.

The quantity used to describe the statistical convergence signal is the *convergence power spectrum*  $P^\kappa(\ell)$ , which is the Fourier transform of the two-point convergence correlation function:

$$\langle \kappa_{\ell m} \kappa_{\ell' m'} \rangle = \delta_{\ell\ell'} \delta_{mm'} P^\kappa(\ell) \quad (5.12)$$

where  $\kappa$  has been expressed in multipole space using the complex conjugated spherical harmonics

$$\kappa_{\ell m} = \int \kappa(\hat{\mathbf{n}}, \chi) Y_{\ell m}^* d\hat{\mathbf{n}}. \quad (5.13)$$

The same derivation cannot be performed for the shear, which is much more easily observed than the convergence. However, in the weak lensing limit, the power spectra of convergence and shear are approximately equal (Huterer, 2010). For this reason, one can use both the connection between convergence and matter density and the observational advantages of shear.

Exploiting the redshift information, the tomographic cross spectrum for redshift bins  $i$  and  $j$  at a given multipole  $\ell$  can be calculated as

$$\langle \kappa_{\ell m, i} \kappa_{\ell' m', j} \rangle = \delta_{\ell\ell'} \delta_{mm'} P_{ij}^\gamma(\ell) \quad (5.14)$$

with  $P_{ij}^\gamma$  being the shear power spectrum.

Since the source galaxies are distributed in a wide range of distances and their properties vary smoothly, the Limber approximation can be used (Bernardeau et al., 2011). This is equivalent to stating that the typical correlation length is smaller than the distance covered with each redshift bin. The approximation means that the 2D angular power spectrum  $P_{ij}^\gamma(\ell)$  can be related to the 3D matter density power spectrum  $P_m$  in the following way, assuming flatness

$$P_{ij}^\gamma(\ell) = \int_0^{\chi_h} \frac{W_i(\chi) W_j(\chi)}{\chi^2} P_m \left( \frac{\ell}{\chi}, z \right) d\chi. \quad (5.15)$$

The matter density power spectrum is the primordial power spectrum  $P(k)$  of eq. (3.35) scaled by a transfer function and a growth function, which evolve the fluctuations (Eisenstein and Hu, 1998). It is possible to define both auto spectra when  $i = j$ , and cross spectra when  $i \neq j$ .

A useful characterization of matter clustering is the root-mean-square amplitude of fluctuations of the present day (matter dominated) power spectrum, on scales of  $8 h^{-1}$  Mpc, called  $\sigma_8$ . This

quantity is roughly 1 today (Ade et al. [Planck Collaboration], 2013).

The statistical uncertainty on the shear power spectrum at each multipole is

$$\sigma_{ij}(\ell) = \sqrt{\frac{2}{2\ell+1} \frac{1}{f_{\text{sky}}}} \left[ P_{ij}^{\gamma}(\ell) + \frac{\langle \gamma_{\text{int}}^2 \rangle}{\bar{n}_i} \right], \quad (5.16)$$

where  $f_{\text{sky}}$  is the fraction of sky area covered by the survey,  $\langle \gamma_{\text{int}}^2 \rangle^{1/2}$  is the rms intrinsic shear and  $\bar{n}_i$  is the average number of galaxies per steradian in the  $i$ th redshift bin;  $\bar{n}_i = \int_0^{\infty} n_i(z) dz$ . The first term in the square brackets comes from cosmic variance of the mass distribution, and is most prominent on large scales (Frieman et al., 2008). The second, shot-noise term represents both the variance in galaxy ellipticities (“shape noise”) and measurement errors caused by noise in the images. Clearly using a high number of galaxies minimizes effects from intrinsic ellipticities. Other errors may include intrinsic correlations of galaxy magnification or shapes, as galaxies may align with their neighbours in a way that can be mistaken for lensing. Finally there may be uncertainties in photometric redshifts and the theoretical matter power spectrum, especially on small scales where non-linearities arise.

Mock auto- and cross spectra for different dark energy parametrizations are shown in fig. [5.2]. The upcoming Euclid mission will perform weak lensing measurements to great precision (Euclid Science Study Team, 2011). Specifications from this survey are used to calculate measurement errors, with

$$\begin{aligned} f_{\text{sky}} &= 0.38, \\ \langle \gamma_{\text{int}}^2 \rangle &= 0.0968, \\ \bar{n}_i &= 30 \text{ galaxies/arcmin}^2 = 3600 \times \left( \frac{180}{\pi} \right)^2 \text{ galaxies/sr}. \end{aligned} \quad (5.17)$$

## 5.2 Supernovae Ia

A type Ia supernova is thought to be the catastrophic thermonuclear explosion of an accreting carbon-oxygen white dwarf in a binary system. The explosion depends on the white dwarf having a specific chemical composition of about 80% oxygen and 20% carbon, which in turns means that the mass of the dwarf will fall into a narrow range around  $\sim 0.6M_{\odot}$  (Rosswog and Brüggen, 2007). The white dwarf cannot become arbitrarily massive as it accretes from its companion star; when it approaches the Chandrasekhar mass of  $1.4M_{\odot}$ , carbon ignites in the center. Since the white dwarf’s electrons are a degenerate gas, their pressure is practically independent of the temperature. The rise in temperature caused by the nuclear reactions is therefore not countered by an increase in the outward pressure, so a further accretion of mass results in a higher and

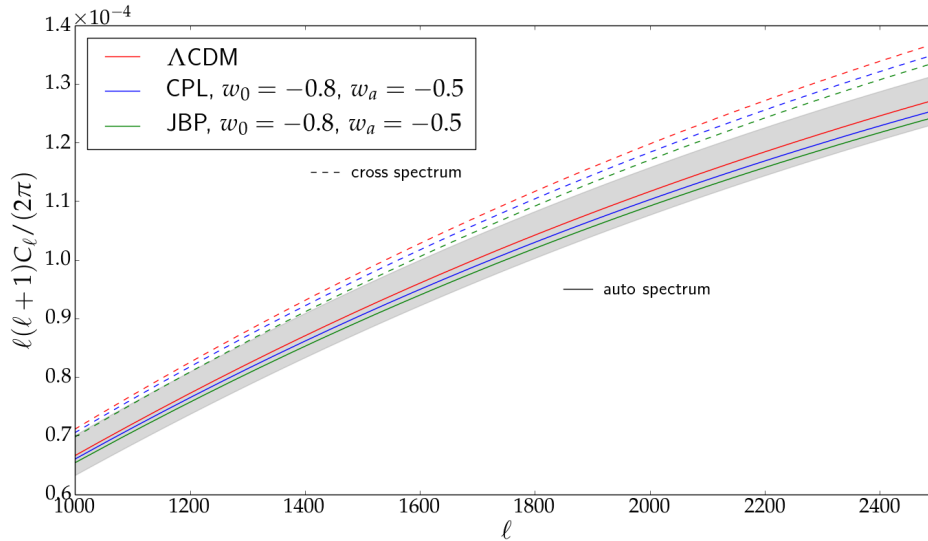


Figure 5.2: Mock shear power spectra as a function of multipole  $\ell$ . Three different dark energy equations-of-state are shown,  $\Lambda$ CDM refers to a cosmological constant  $w_{\text{DE}} = -1$ . Solid lines are auto spectra of the bin with redshift ranges  $1.03117 \leq z \leq 1.16347$ . Dashed lines are cross spectra between this bin and the bin with ranges  $1.16348 \leq z \leq 1.31141$ . The shading represents the  $1\sigma$  uncertainty on the auto spectrum of the  $\Lambda$ CDM model, and is similar to the uncertainties on the other models and cross spectra.

higher central temperature. At some point, the energy generation rate exceeds the rate at which energy can be carried away as heat. A thermonuclear runaway process sets in, beginning with the burning of carbon and oxygen and ending in primarily nickel and cobalt. The explosion can be as bright as an entire galaxy, making SNe Ia excellent objects to study.

Because white dwarfs have nearly the same mass before exploding, and because they are all degenerate electron gasses with the same explosion mechanism, SNe Ia display very similar luminosities as a function of time, or light curves. These are the result of radioactive decays of  $^{56}\text{Ni}$  at early times and  $^{56}\text{Co}$  at late times. The peak luminosity is determined by the amount of  $^{56}\text{Ni}$  produced in the explosion, which for a fully burned white dwarf is about 0.6 solar masses. Though some white dwarfs may not be completely burned, and the explosion mechanism is still not fully understood, the majority of SNe Ia do exhibit similar light curves. Since their intrinsic luminosities are the same, their apparent luminosities must be a result of their distances from us.

The apparent magnitude  $m$  is used as an observational measure of the apparent luminosity.

The difference between the apparent and absolute magnitudes is known as the *distance modulus*  $\mu \equiv m - M$ . This can be related to the luminosity distance  $d_L$  in the units of parsecs (Frieman et al., 2008):

$$d_L = 10^{\mu/5+1}. \quad (5.18)$$

Observing both  $d_L$  and the supernova's corresponding scale factor at the time of emission, the expansion history of the universe can be probed.

The luminosity distance is cosmology-dependent. Its definition is

$$d_L(z) \equiv \sqrt{\frac{L}{4\pi F}} = (1+z)\chi, \quad (5.19)$$

where  $L$  is the luminosity,  $F$  the received flux and  $\chi$  the comoving distance to the object. The cosmology-dependence is contained in the comoving distance as shown in eq. (3.31). Setting the two expressions for  $d_L$  equal yields  $\mu(z)$ .

Observations of SNe Ia are complicated by the fact that they are not intrinsically standard candles. There is an empirical correlation between the peak luminosity and the rate of dimming, so that brighter SNe Ia have light curves which decline more slowly. This should be accounted for by “stretching” the light curve (Frieman et al., 2008).

There are also observational difficulties in accurately determining the apparent luminosities. The host galaxy may contain dust, which causes extinction, and there are variations in intrinsic SN Ia colors. These effects can, however, be minimized with multiband observations, and particularly near-infrared observations suffer less from extinction.

Furthermore, the templates of light curves are based on low-redshift SNe Ia, and though the sample contains objects with different galactic environments, it may be too heterogeneous to be readily applied to the high-redshift counterparts. Finally, it is still unclear whether the peak luminosity correlates with such factors as host galaxy type, binary system evolution and metallicity.

Following the method of Cardone et al. (2012) to obtain the number of usable SNe Ia and their redshift distribution, mock data are produced in the form of  $\mu(z)$ . The standard deviation can then be expressed as

$$\sigma_\mu(z) = \sqrt{\sigma_{\text{sys}}^2 + (z/z_{\text{max}})^2 \sigma_m^2}, \quad (5.20)$$

where  $\sigma_{\text{sys}}$  is an irreducible systematic scatter,  $z_{\text{max}}$  the maximum redshift of the sample and  $\sigma_m$  depends on the photometric accuracy in determining the apparent luminosity. Typical values for

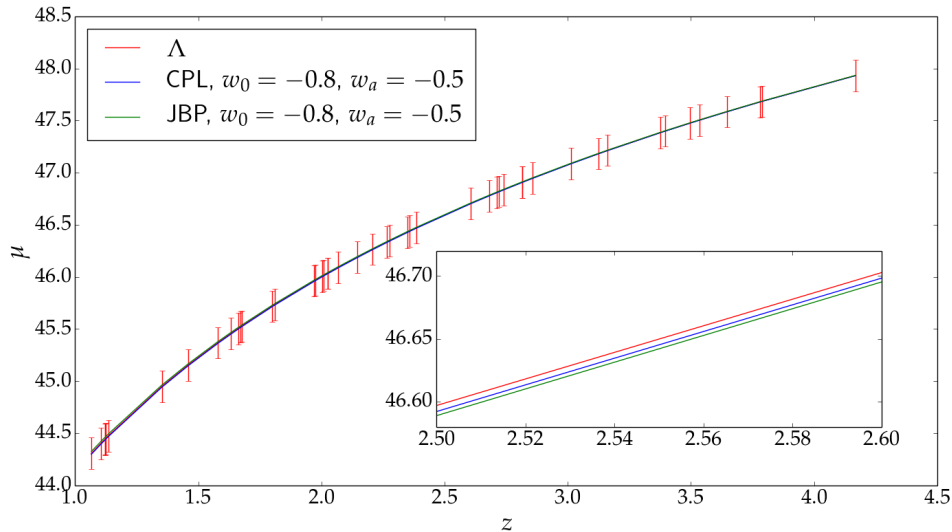


Figure 5.3: Mock SNe Ia distance moduli  $\mu$  as a function of redshift, shown for three different cosmological models. Errors are shown for the  $\Lambda$ CDM model and are identical to those of the CPL and JBP models. The three models are extremely similar, but the insert makes it possible to distinguish between them.

a space based survey are

$$\begin{aligned}
 z_{\max} &= 1.4, \\
 \sigma_{\text{sys}} &= 0.15, \\
 \sigma_m &= 0.02.
 \end{aligned}
 \tag{5.21}$$

Figure [5.3] shows the SN Ia mock data for different dark energy equations-of-state.

### 5.3 Redshift drift

Redshift drift is a term for the change in redshift of a source over time. Since the universe expands, measurements of a single source at different times will yield slightly different redshifts. The first person to suggest this type of survey was Allan Sandage, who in 1962 calculated the possibility of detecting such a signal (Sandage, 1962). With the technology available at the time, the tiny changes in redshift required measurements separated by periods of  $10^7$  years. Fortunately, the technology has since improved. In 1998 Abraham Loeb revisited the idea and suggested using spectroscopic redshifts of the Ly $\alpha$  forests of distant quasars (QSOs), as these bright sources have sharp spectral features and small peculiar motions (Loeb, 1998). With the redshift drift estimated to be a few m/s each century, the signal should be detectable with observations set a

few decades apart.

Redshift drift has the advantage of being a direct probe of cosmic evolution. The physics behind it is simple and well-understood, and the only assumptions necessary are large scale isotropy and homogeneity. Furthermore, suitable candidate QSOs can be found at a redshift of  $2 \leq z \leq 5$  using the high-resolution CODEX spectrograph (Bonifacio et al. [CODEX], 2010). This redshift region is traditionally poorly probed, as e.g. SNe Ia and weak lensing probe smaller redshifts and the CMB much higher.

Consider a source at redshift  $z$ . Let  $t_s$  be the time of electromagnetic wave emission and  $t_0$  the time of observation. The cosmological redshift as measured by the observer is given by eq. (3.4):

$$1 + z(t_0) = \frac{a(t_0)}{a(t_s)}. \quad (5.22)$$

Now consider a second wave emitted at a later time  $t_s + \Delta t_s$  and detected at  $t_0 + \Delta t_0$ . The observed redshift will then be

$$1 + z(t_0 + \Delta t_0) = \frac{a(t_0 + \Delta t_0)}{a(t_s + \Delta t_s)}. \quad (5.23)$$

The observed difference in redshift  $z(t_0 + \Delta t_0) - z(t_0)$  is thus

$$\Delta z \equiv \frac{a(t_0 + \Delta t_0)}{a(t_s + \Delta t_s)} - \frac{a(t_0)}{a(t_s)} \quad (5.24)$$

In the limit  $\Delta t \ll t$ , the scale factor can be expanded to linear order,  $a(t + \Delta t) \approx a(t) + \dot{a}\Delta t$ . From eq. (5.22) the relation  $\Delta t_0/\Delta t_s = a(t_0)/a(t_s)$  can be obtained, hence the difference in redshift can be expressed as (Loeb, 1998)

$$\Delta z \approx \left( \frac{\dot{a}(t_0) - \dot{a}(t_s)}{a(t_s)} \right) \Delta t_0. \quad (5.25)$$

It is convenient to express the redshift drift in terms of the spectroscopic velocity shift  $\Delta v$ :

$$\frac{\Delta v}{c} \equiv \frac{\Delta z}{1 + z}. \quad (5.26)$$

Using again the quantity  $E(z)$  as derived from the Friedmann equation (eq. (3.29)) and setting  $a(t_0) = 1$ , the velocity shift  $\Delta v$  and the time between observations  $\Delta t_0$  can be related to the

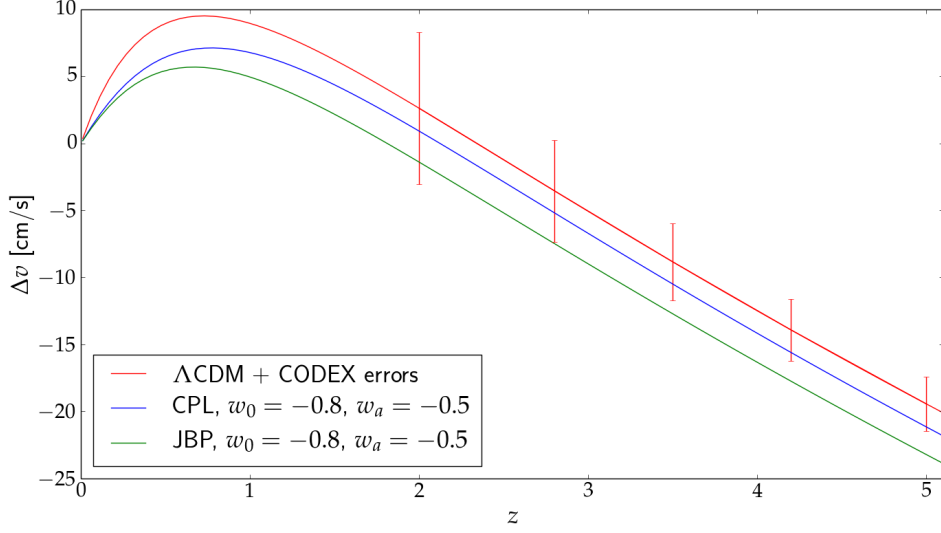


Figure 5.4: Mock velocity shifts as a function of source redshift for three different cosmological models. Error bars are made for the CODEX instrument for five different redshifts and in accordance with eq. (5.28).

cosmological model:

$$\frac{\Delta v}{c} = H_0 \Delta t_0 \left[ 1 - \frac{E(z)}{1+z} \right]. \quad (5.27)$$

According to Monte Carlo simulations carried out in connection with the high-resolution spectrograph of the European Extremely Large Telescope CODEX, the error on the measured spectroscopic velocity shift  $\Delta v$  can be expressed as (Bonifacio et al. [CODEX], 2010)

$$\sigma_{\Delta v} = 1.35 \frac{2370}{S/N} \sqrt{\frac{30}{N_{\text{QSO}}}} \left( \frac{5}{1+z_{\text{QSO}}} \right)^x \text{ cm s}^{-1}, \quad (5.28)$$

where  $S/N$  is the signal-to-noise ratio,  $N_{\text{QSO}}$  the number of QSOs,  $z_{\text{QSO}}$  the redshift and

$$x = \begin{cases} 1.7 & \text{if } z_{\text{QSO}} \leq 4 \\ 0.9 & \text{if } z_{\text{QSO}} > 4 \end{cases}. \quad (5.29)$$

Figure [5.4] shows the velocity shift for different cosmological models. Following Martinelli et al. (2012), values of  $S/N = 3000$ ,  $N_{\text{QSO}} = 6$  and  $\Delta t = 30$  years have been adopted.

## 6 Method

Since altering the dark energy equation-of-state affects observable values as shown in section 5, it will also affect the cosmological parameter values obtained by fitting equations to those observable values. In this section the method used to calculate the effect will be discussed.

Mock data are produced to simulate *fiducial* cosmologies. The mock data are then fitted with a *framework* cosmology providing the specific forms of the cosmological equations. In this way, marginalized posterior probability distributions, i.e. expectation values and uncertainties, are obtained for each cosmological parameter. A schematic diagram of the method can be seen in fig. [6.1].

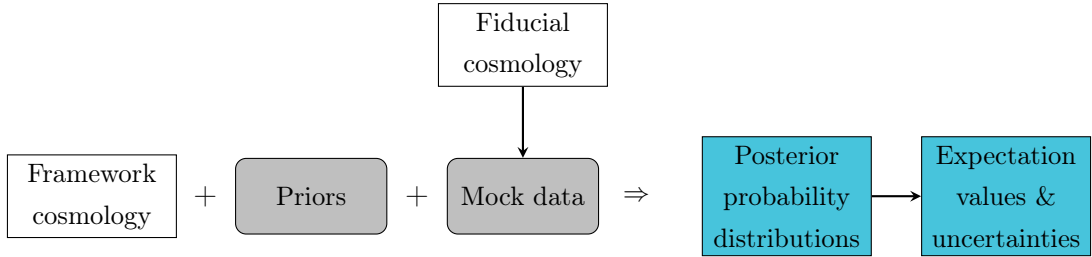


Figure 6.1: Diagram showing the method of obtaining marginalized posterior probability distributions/expectation values and errors when analyzing a fiducial cosmology with a framework cosmology.

The goal of this analysis is to investigate how well the framework model can recover the fiducial values of the cosmological parameters used to create the mock data. Alternatively, one could ask whether the choice of a specific  $w_{\text{DE}}$  in the framework cosmology causes a bias in parameter determination when the choice does not match the fiducial cosmology. Quantitatively this can be expressed by the *shift*:

$$\frac{\Delta}{\sigma} = \frac{|\phi_i - \phi_i^{fid}|}{\sigma_i} . \quad (6.1)$$

Here  $\phi_i$  is the mean value of the  $i$ th cosmological parameter as obtained through analysis,  $\sigma_i$  is the corresponding standard deviation and  $\phi_i^{fid}$  is the fiducial value of the parameter. A shift larger than 1 will thus signify that the recovered mean value is farther than  $1\sigma$  away from the input fiducial value.

Both mock data production and cosmological parameter estimations are done with the Markov Chain Monte Carlo engine CosmoMC (Lewis, 2012). The default program is modified by Matteo

Martinelli and Stefania Pandolfi to accommodate a redshift-dependent dark energy equation-of-state.

The statistical foundation and calculation of marginalized posterior probability distributions will be discussed first, followed by a section focusing on the production of mock data.

## 6.1 Bayesian inference

In cosmology it is often a challenge to estimate a theoretical model's parameter values from observational data. For doing so one can use the tools of Bayesian inference. This method of parameter estimation expresses the parameters and their uncertainties in terms of probability.

First, let  $\boldsymbol{\theta} = (\theta_1, \theta_2, \dots, \theta_M)$  be the vector of  $M$  model parameters, which reflect the qualitative knowledge of a physical system, e.g. the expansion history of the universe. Examples of elements in  $\boldsymbol{\theta}$  are  $\Omega_b h^2$  or  $n_S$ .

Let  $\mathbf{x} = (x_1, x_2, \dots, x_N)$  be the  $N$ -dimensional vector containing the measurement values of a data set, e.g. the luminosity distances to  $N$  supernovae type Ia.  $\mathbf{x}$  is thus a random variable which depends in some known way on the vector  $\boldsymbol{\theta}$ .

The probability for the theoretical model's parameters to take on a certain set of values  $\boldsymbol{\theta}$ , given the experimental data  $\mathbf{x}$ , can be written as (Hobson et al., 2010)

$$p(\boldsymbol{\theta}|\mathbf{x}). \quad (6.2)$$

This is called the *posterior probability*, as it expresses the probability of a certain parameter state after doing the experiments.

Unfortunately, the posterior distribution is rarely straightforward to find. Instead, one may turn the problem around: if we assume that the universe is built with a certain cosmology, what would the observations look like? In other words: if  $\boldsymbol{\theta}$ , then how probable is each  $x$ ; or, what is  $p(x|\boldsymbol{\theta})$ ? Note that the observational value is now a scalar and only refers to one data point.

In the simple case of a Gaussian distribution of  $x$ , the two parameters that completely determine  $p(x|\boldsymbol{\theta})$  are the mean  $\mu$  and the variance  $\sigma^2$ :

$$p(x|\boldsymbol{\theta}) = \frac{1}{\sqrt{2\pi}\sigma} \exp\left[-\frac{(x-\mu)^2}{2\sigma^2}\right]. \quad (6.3)$$

This quantity is known as the *likelihood*. To avoid confusion with the posterior distribution, it may be written as  $L(\mathbf{x}; \boldsymbol{\theta})$ . The  $\sigma^2$  appearing here is not the same as used in describing the shift in eq. (6.1); rather, it is the error made in measuring  $\mathbf{x}$ .

Bayesian inference makes use of Bayes' theorem (Bayes and Price, 1763) to exploit the knowl-

edge of  $p(\mathbf{x}|\boldsymbol{\theta})$  to find  $p(\boldsymbol{\theta}|\mathbf{x})$ :

$$p(\boldsymbol{\theta}|\mathbf{x}) = \frac{p(\mathbf{x}|\boldsymbol{\theta})p(\boldsymbol{\theta})}{p(\mathbf{x})}. \quad (6.4)$$

Here  $p(\boldsymbol{\theta})$  is the *prior probability*, which expresses what we know about  $\boldsymbol{\theta}$  before performing the experiment. One may have constraints on a parameter from a previous experiments, or perhaps a parameter is physically limited - either way, we assume that this a priori information can be expressed in terms of probability. The subtle switch from  $p(x|\boldsymbol{\theta})$  to  $p(\mathbf{x}|\boldsymbol{\theta})$  signifies the inclusion of all data points in a data set.

The final quantity,  $p(\mathbf{x})$ , is called the *evidence*. This is a normalizing factor;

$$p(\mathbf{x}) = \int p(\mathbf{x}|\boldsymbol{\theta})p(\boldsymbol{\theta}) d\boldsymbol{\theta}. \quad (6.5)$$

The evidence is identical for all parameters of a model, so it is often left out.

When dealing with just one model, then,

$$p(\boldsymbol{\theta}|\mathbf{x}) \propto L(\mathbf{x}; \boldsymbol{\theta})p(\boldsymbol{\theta}). \quad (6.6)$$

Turning again to the prior, one notices that if a parameter is equally likely to take on any value (“flat priors”), the prior is also identical for all calculations of the posterior. In this case,

$$p(\boldsymbol{\theta}|\mathbf{x}) \propto L(\mathbf{x}; \boldsymbol{\theta}). \quad (6.7)$$

Since the full posterior probability distribution is not always attainable or even analytical, one can estimate the parameters using only the peak of the distribution. This is called a *maximum likelihood* estimate. Comparing eq. (6.6) and eq. (6.7), it is clear that in general, the peak in the posterior distribution only matches the maximum likelihood if the priors are flat.

To sum up; in order to calculate the posterior probability distribution for a single model, one needs the likelihood and the prior. The latter is decided upon, and there may be differing opinions about it. It may also affect the results. The likelihood depends on the data and is calculated in CosmoMC using Monte Carlo Markov Chains, which is the subject of the following section.

## 6.2 Monte Carlo Markov Chains

A cosmological model may contain a large number of parameters, all of which can take on different values. This means that evaluating the likelihood becomes hard work, as the number of grid points in parameter space grows exponentially with its dimension (Lewis and Bridle, 2002). It is therefore often advantageous to sample the likelihood, preferably in a way which samples the high likelihood regions more intensely. One method of doing this is Monte Carlo Markov Chains.

Monte Carlo algorithms rely on repeated random sampling to obtain distributions of unknown entities, in this case the model parameters. There are several ways of obtaining the samples; one of the most widely used and versatile ones is the Markov Chains method (Hobson et al., 2010). A Markov chain is a way of exploring the parameter space by moving from one state  $\boldsymbol{\theta}_1$  (set of specified values for all parameters) to another  $\boldsymbol{\theta}_2$ . It is 'memoryless' in the sense that the move to a new state depends only on the current one, and not on any previous states. For each state, the likelihood is evaluated by comparing the state  $\boldsymbol{\theta}$  to the data set  $\mathbf{x}$ . The decision of whether to transition to a new state is then determined probabilistically on the basis of the posteriors. For notational simplicity, posteriors will be expressed as  $P$  in this section.

The simplest way of sampling in this way is the Metropolis-Hastings algorithm. This has a transition kernel between states  $T(\boldsymbol{\theta}_n, \boldsymbol{\theta}_{n+1})$  chosen so that the Markov chain converges to the true posterior distribution of parameters,  $P(\boldsymbol{\theta})$  (Lewis and Bridle, 2002). Formally, the requirement of detailed balance must be met:

$$P(\boldsymbol{\theta}_{n+1})T(\boldsymbol{\theta}_{n+1}, \boldsymbol{\theta}_n) = P(\boldsymbol{\theta}_n)T(\boldsymbol{\theta}_n, \boldsymbol{\theta}_{n+1}). \quad (6.8)$$

By expressing the transition kernel as the product of an acceptance probability  $\alpha$  and a proposal density  $q$ ;

$$T(\boldsymbol{\theta}_n, \boldsymbol{\theta}_{n+1}) = \alpha(\boldsymbol{\theta}_n, \boldsymbol{\theta}_{n+1})q(\boldsymbol{\theta}_n, \boldsymbol{\theta}_{n+1}), \quad (6.9)$$

and choosing the acceptance probability to be of the form

$$\alpha(\boldsymbol{\theta}_n, \boldsymbol{\theta}_{n+1}) = \min \left[ 1, \frac{P(\boldsymbol{\theta}_{n+1})q(\boldsymbol{\theta}_{n+1}, \boldsymbol{\theta}_n)}{P(\boldsymbol{\theta}_n)q(\boldsymbol{\theta}_n, \boldsymbol{\theta}_{n+1})} \right], \quad (6.10)$$

detailed balance is indeed ensured.

If the proposal density  $q$  is symmetric, the acceptance probability is simplified to

$$\alpha(\boldsymbol{\theta}_n, \boldsymbol{\theta}_{n+1}) = \min \left[ 1, \frac{P(\boldsymbol{\theta}_{n+1})}{P(\boldsymbol{\theta}_n)} \right]. \quad (6.11)$$

Furthermore, the proposal density should be chosen in a way that prevents the chain from getting stuck in one region of parameter space.

The Monte Carlo Markov Chains method works in the following way, then:

1. Choose a starting state.
2. Propose a random jump from the current state  $\boldsymbol{\theta}_n$  to a candidate state  $\boldsymbol{\theta}_{n+1}$ . The candidate is proposed from the proposal density  $q$ , whose symmetry means that a jump from  $\boldsymbol{\theta}_n$  to  $\boldsymbol{\theta}_{n+1}$  is precisely as probable as the reverse jump. A common symmetrical function to use is a multivariate Gaussian about  $\boldsymbol{\theta}_n$ .
3. Evaluate the likelihood at  $\boldsymbol{\theta}_{n+1}$  and multiply by the prior for that state to obtain the posterior probability  $P(\boldsymbol{\theta}_{n+1})$ .

4. Accept the candidate  $\theta_{n+1}$  as the next state with the probability given by eq. (6.11). If the posterior probability of the candidate state is larger than that of the current state, the jump will always be accepted. If it is lower, however, the jump will still be accepted with a probability of  $\frac{P(\theta_{n+1})}{P(\theta_n)}$ . This ensures that the region around a very high likelihood will also be explored. If the jump is not accepted, the chain stays at  $\theta_n$  and creates a duplicate of it.
5. Repeat until the entire posterior probability distribution is well-sampled.

Starting a chain in a random position in parameter space means that it takes a little time to equilibrate to sampling from the posterior distribution rather than being influenced by the starting point. This is known as the burn-in. After that phase, each chain element will be a correlated sample from the posterior. To lessen the correlation, one can thin the chain, giving it time to move to an uncorrelated state.

There are different ways of making sure that the posterior distribution is well-sampled. One of the most common ones is the Gelman-Rubin convergence diagnostic (Gelman and Rubin, 1992), which requires at least two chains. For each chain, one must first discard the burn-in. The Gelman-Rubin method then consists of comparing the 'within-chain variance'; treating each chain separately, with the 'between-chain variance'; treating all chains as a single one. If the chains have converged, these two entities should agree to within some tolerance. Quantitatively, this means that the ratio between the two variances, the so-called 'potential scale reduction factor'  $R$ , should not exceed 1 by more than a certain amount. It is common to express convergence in terms of  $R - 1$ .

Once the sample of the posterior distribution has been obtained one can, for each cosmological parameter, average over all other parameters to estimate the marginalized posterior probability distribution.

The Monte Carlo Markov Chains method of course requires data sets to calculate the likelihood from. Producing the mock data is the subject of the following section.

### 6.3 Mock data

Mock data are synthetic data sets built according to the specifications of particular experiments. The calculated observable values are cosmology-dependent as shown in section 5. Simulating data in this way allows one to completely control the fiducial cosmology and hence quantify the possible effect of assuming a specific dark energy equation-of-state parametrization on the recovered cosmological parameter values. Furthermore, using the experimental specifications to calculate the observable values and errors allows one to test the sensitivity of future high-precision

Bin	$z$	Bin	$z$
1	0 - 0.49595	6	1.03117 - 1.16347
2	0.49596 - 0.65371	7	1.16348 - 1.31141
3	0.65372 - 0.78448	8	1.31142 - 1.50210
4	0.78449 - 0.90731	9	1.50211 - 1.78240
5	0.90732 - 1.03116	10	1.78241 - 5.0

Table 6.1: Redshift ranges of the ten bins used for weak lensing mock data.

observations. Mock data are made for a cosmological constant model and a JBP model. Weak lensing, supernovae type Ia and redshift drift are chosen as observational probes. The analysis is carried out using different combinations of the probes to investigate the impact of the experimental configuration on the results.

The source code of CosmoMC is modified to output files of redshifts and observable values for the three probes when running. By fixing the prior values of the cosmological parameters to their fiducial values, the program is no longer free to move around in parameter space. The outputted observable values are then simply what would be seen in a universe with completely known cosmological parameter values. These can therefore be used as mock data. The modifications are partially made by Matteo Martinelli and Stefania Pandolfi.

Tomographic weak lensing shear spectra are calculated according to eq. (5.15) for multipole numbers 1 to 2500. 10 redshift bins are used, with each bin containing an equal number of galaxies. The redshift ranges of the bins are shown in table 6.1. Specifications from the Euclid survey (Euclid Science Study Team, 2009) are used to calculate simulated errors as in section 5.1.

For SNe Ia, distance moduli (eq. (5.18) and eq. (5.19)) and simulated experimental errors (eq. (5.20)) are calculated as a function of 48 different redshifts in the range  $z \in [1.066, 4.169]$ . The redshift distribution is obtained following the method of Cardone et al. (2012).

Finally, velocity shifts are calculated for five different redshift bins with six QSOs each to constitute the redshift drift mock data (eq. (5.27)), following the choices of Martinelli et al. (2012). A time difference of  $\Delta t = 30$  years is chosen, and simulated errors are calculated as described in section 5.3 to mimic the spectroscopy of the CODEX instrument (Bonifacio et al. [CODEX], 2010).

Having produced the mock data sets the Monte Carlo Markov Chains analysis can be performed. The following section discusses the results obtained.

## 7 Results & Discussion

The goal of this work is to quantify the error made when assuming a dark energy parametrization which cannot reproduce the actual dark energy behaviour. A CPL framework cosmology is used to analyze mock data derived from a cosmological constant and a JBP dark energy equations-of-state. In accordance with customary assumptions and simplifications space-time is assumed to be flat; the universe is assumed to consist only of baryons, dark matter and dark energy; the spectral index of primordial perturbations  $n_S$  is assumed to be a constant; and tensor perturbations are assumed to be vanishingly small.

A prior top-hat function is used to constrain the age of the universe to be between 10 and 20 Gyr. Chains are stopped once a convergence of  $R - 1 \leq 0.03$  has been reached.

An overview of the different analysis configurations is shown in table 7.1. Different combinations of probes are used to showcase their constraining powers. Throughout this section, the cosmological constant fiducial model will be referred to as “ $\Lambda$ CDM”.

Case	Fiducial cosmology	Probe(s)
1	$\Lambda$ CDM	WL
2	$\Lambda$ CDM	SN Ia + RD
3	$\Lambda$ CDM	WL + SNe Ia + RD
4	JBP	SNe Ia + RD
5	JBP	WL + SNe Ia + RD

Table 7.1: Overview of analyses. “Probe(s)” defines the kind(s) of mock data used. All cases use a CPL framework cosmology.

The fiducial values used to construct the mock data are, with the exception of the dark energy parameters, the mean values of the WMAP9  $\Lambda$ CDM analysis (Hinshaw et al. [WMAP], 2013). For the JBP fiducial model,  $w_0$  and  $w_a$  are chosen to be within the  $2\sigma$  range of results obtained by Jassal et al. (2005) while being allowed to differ significantly from a  $\Lambda$ CDM cosmology. The values are chosen specifically to preserve the Dominant Energy Condition and thereby avoid the phantom region. All fiducial values are listed in table 7.2.

The mock data are analyzed with a framework cosmology, yielding marginalized posterior probability distributions. Mean values and uncertainties are given in table 7.3 and table 7.4 along with the shifts  $\Delta/\sigma$  defined in eq. (6.1). Only results for parameters relating directly to dark energy or the expansion history are shown. A full table of results can be found in the appendix.

The following sections will discuss each case separately.

Parameter		Fiducial value
$\Omega_b h^2$	Physical baryon density	0.02264
$\Omega_{\text{DM}} h^2$	Physical dark matter density	0.1138
$\theta$	Acoustic scale, $r_s(z_*)/d_A$	1.0391
$\tau$	Optical depth at reionization	0.089
$n_S$	Spectral index of primordial perturbations	0.972
$\log(10^{10} A_S)$	Amplitude of primordial power spectrum	3.18
$w, \Lambda\text{CDM}$	Dark energy (DE) parameter, $\Lambda\text{CDM}$	-1
$w_0, \text{JBP}$	Present day DE parameter, JBP	-0.8
$w_a, \text{JBP}$	Time-varying DE parameter, JBP	-0.5
$\Omega_m, \Lambda\text{CDM}$	Matter energy density (baryons and dark matter)	0.2800
$\Omega_m, \text{JBP}$		0.3138
$H_0, \Lambda\text{CDM}$	Hubble constant	69.80 km/s/Mpc
$H_0, \text{JBP}$		65.94 km/s/Mpc
$\sigma_8, \Lambda\text{CDM}$	rms amplitude of mass fluctuations at $8 h^{-1}$ Mpc	0.8243
$\sigma_8, \text{JBP}$		0.7873

Table 7.2: List of parameters for which marginalized posterior probabilities are obtained. The rightmost column are the values used to produce mock data. Parameters below the horizontal line are derived from those above it.

## 7.1 $\Lambda\text{CDM}$ fiducial cosmology

$\Lambda\text{CDM}$  mock data is analyzed using a CPL framework cosmology. Since the  $\Lambda\text{CDM}$  cosmology can be reproduced by the CPL model (with  $w_0 = -1$ ,  $w_a = 0$ ), the latter is expected to recover the fiducial values well, though some statistical noise is assumed to appear.

### 7.1.1 Case 1: weak lensing

Plots of the marginalized posterior probability distributions of case 1 are shown in fig. [7.1]. Red vertical lines show the fiducial values of table 7.2, while blue lines represent the recovered distributions.

Weak lensing constrains the parameters  $\Omega_m$  and  $H_0$  through the weighting equation (eq. (5.9)) and  $\sigma_8$  through the matter density power spectrum. Their distributions show mean values consistent with the fiducial ones;  $\Omega_m$  ( $0.2797 \pm 0.001123$ ) and  $\sigma_8$  ( $0.8245 \pm 0.001400$ ) show shifts  $\Delta/\sigma$  of 0.2492 and 0.1673, respectively, while  $H_0$  ( $69.84 \pm 0.5708$ ) has a shift of the order of  $10^{-2}$ . All shifts are well below 1, hence the recovered values are within 1 standard deviation of the fiducial ones. The shifts can therefore be ascribed to the statistical nature of the Monte

Carlo Markov Chains parameter estimation technique.

The dark energy parameters  $w_0$  ( $-1.002 \pm 0.01193$ ) and  $w_a$  ( $0.003327 \pm 0.04625$ ) are similarly well-recovered with shifts of  $10^{-2} - 10^{-3}$ , as expected.

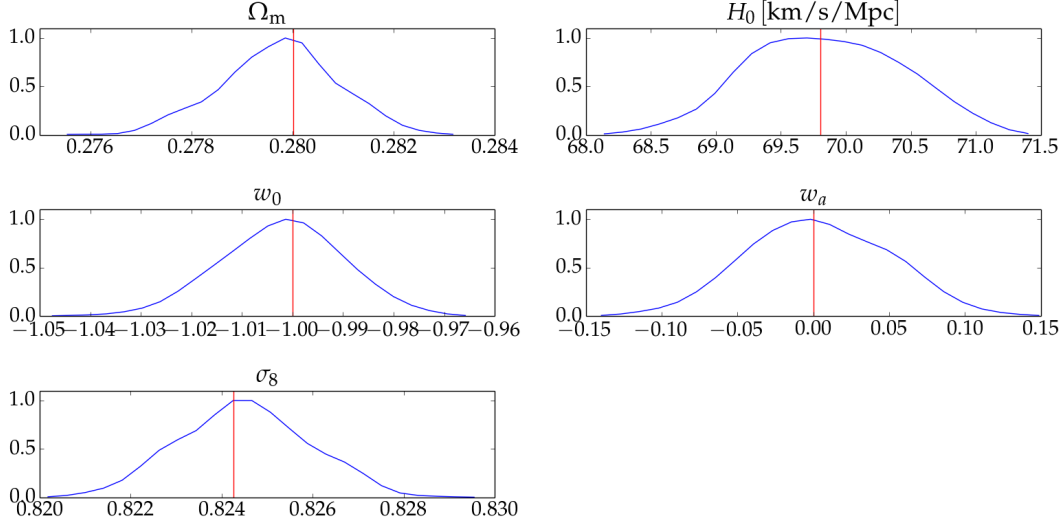


Figure 7.1: Marginalized posterior probability distributions of case 1:  $\Lambda$ CDM fiducial cosmology, CPL framework cosmology, using only WL. Red lines indicate fiducial values used to produce the mock data.

### 7.1.2 Case 2: supernovae Ia & redshift drift

Using the other two types of mock data, SN Ia and RD, yields the marginalized posterior distributions of fig. [7.2]. Since weak lensing has been removed as a probe  $\sigma_8$  is no longer calculated.

SNe Ia constrain both  $\Omega_m$ ,  $H_0$ ,  $w_0$  and  $w_a$  through the comoving distance in eq. (5.19), while redshift drift constrains the same parameters through eq. (5.27).

$w_a$  shows a large probability for a wide range of values, and the distribution is quite abruptly cut off at the sides. The program CosmoMC requires priors in the form of mean -, lower - and upper values, and the recovered distribution here simply shows a high probability of most values within the starting range  $[-2.0, 2.0]$ , dropping off rapidly outside it.

The standard deviations of case 2 are between 3 and 21 times larger than those of case 1, suggesting that SNe Ia and RD are less effective than weak lensing at constraining the cosmological parameters.

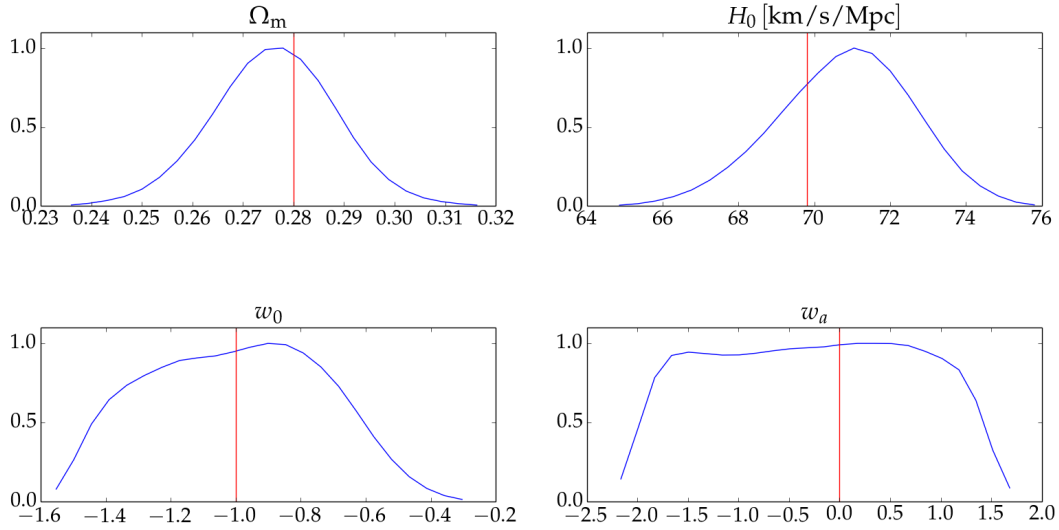


Figure 7.2: Marginalized posterior probability distributions of case 2:  $\Lambda$ CDM fiducial cosmology, CPL framework cosmology, using SNe Ia and RD. Red lines indicate fiducial values used to produce the mock data. Notice that  $\sigma_8$  is not calculated, since weak lensing data are not included.

From table 7.3 it is evident that the shifts of  $\Omega_m$  (0.3264),  $H_0$  (0.5673) and  $w_a$  (0.2748) are all larger than their counterparts of case 1. The small shift of  $w_0$  ( $3.507 \times 10^{-3}$ ) is caused by the standard deviation being very large (0.2615 compared to 0.01193 in case 1), and is hence not a result of the constraining power of SNe Ia and RD. However, since the shifts in both cases are within  $1\sigma$  from the fiducial values, the ratio of the shifts of the two cases is of minor importance.

### 7.1.3 Case 3: weak lensing, supernovae Ia & redshift drift

The results of combining all three probes can be seen in the marginalized posterior probability distributions in fig. [7.3]. The fiducial values are recovered nicely, with all shifts being below 1 as in the previous two cases.

Figure [7.4] shows the marginalized posterior probability distributions of cases 1 (green lines), 2 (yellow lines) and 3 (blue lines) together for comparison. It is apparent that weak lensing is especially useful in determining the dark energy parameters to great precision.

The standard deviations of case 3 are very similar to those of case 1. This indicates that the precision is not increased by using all three probes together, although the mean value may be shifted. This is seen most clearly in  $H_0$  ( $69.96 \pm 0.6168$ ) which has a standard deviation only 1.1 times that of case 1, yet still shows a shift 3.7 times larger.

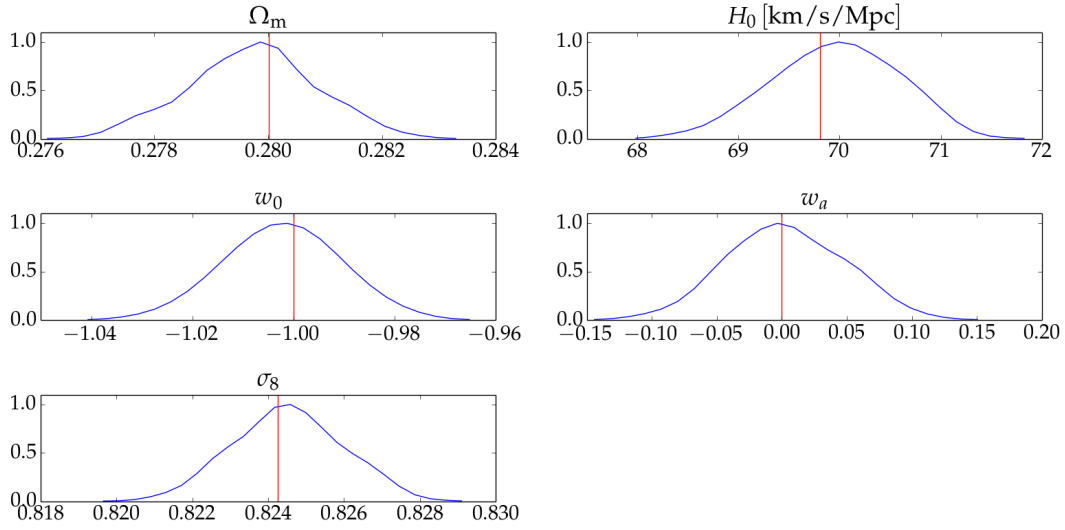


Figure 7.3: Marginalized posterior probability distributions of case 3:  $\Lambda$ CDM fiducial cosmology, CPL framework cosmology, using all probes (WL, SNe Ia and RD). Red lines indicate fiducial values used to produce the mock data.

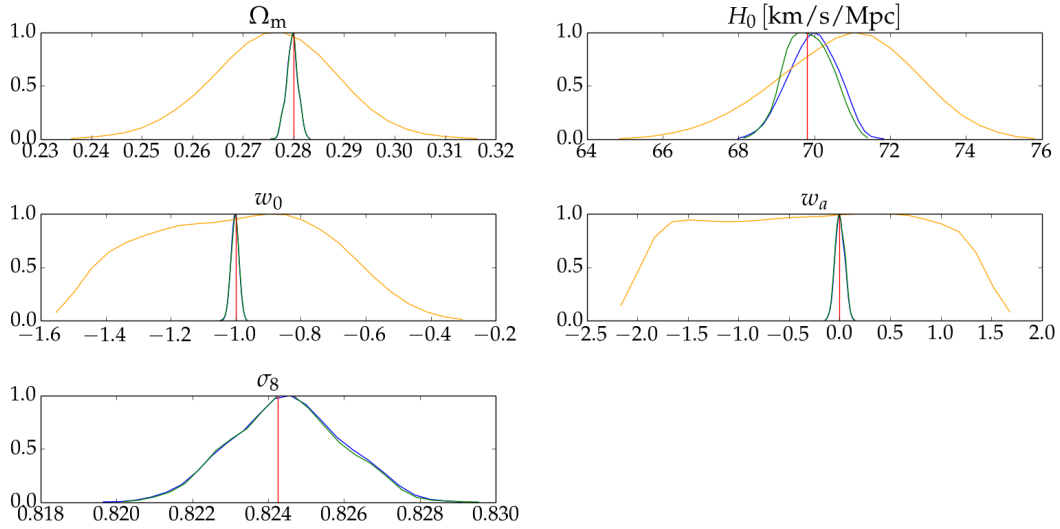


Figure 7.4: Marginalized posterior probability distributions of cases using a  $\Lambda$ CDM fiducial cosmology. Green lines show case 1 (WL only), yellow lines case 2 (SNe Ia + RD) and blue lines case 3 (WL + SNe Ia + RD).

Plotting the 1- and  $2\sigma$  confidence regions in the parameter subspace spanned by the two parameters  $H_0$  and  $\Omega_m$  results in fig. [7.5], where the green figure represent case 1 using only WL and the yellow figure case 2 using SNe Ia and RD. The confidence regions of cases 1 and 2 have different orientations in the  $H_0 - \Omega_m$  plane. Hence, if a weak lensing experiment were to yield larger standard deviations on either  $\Omega_m$  or  $H_0$  than what is shown here, the data could be combined with SNe Ia and redshift drift data to tighten the constraints. However, since the constraints on both parameters in this analysis are tighter in the case using weak lensing, combining all three probes will not improve the results, c.f. fig. [7.6].

The results of these three cases verify that the CPL model is able to recover the  $\Lambda$ CDM cosmology.

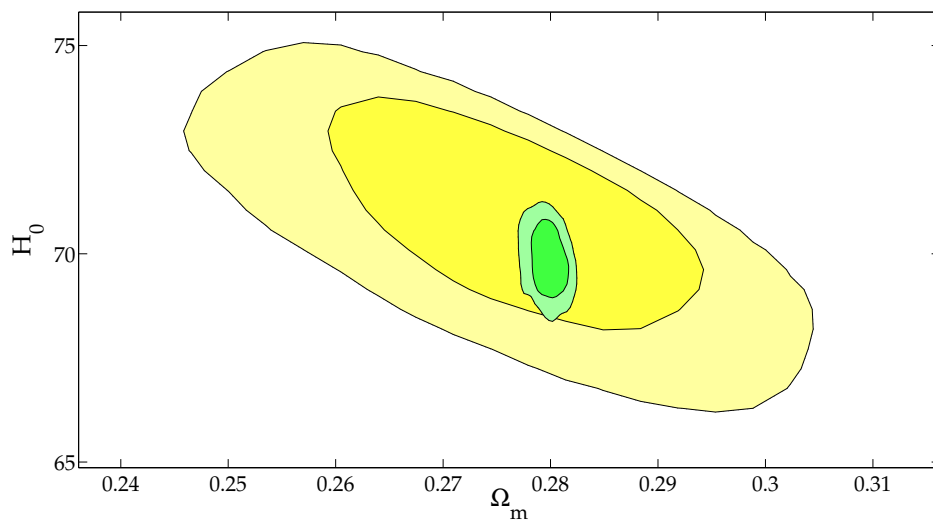


Figure 7.5: 1- and  $2\sigma$  confidence regions in the parameter space of  $\Omega_m$ ,  $H_0$ . The green figure represents case 1 (using only WL) and the yellow figure case 2 (using SNe Ia + RD). Both cases use a  $\Lambda$ CDM fiducial cosmology.

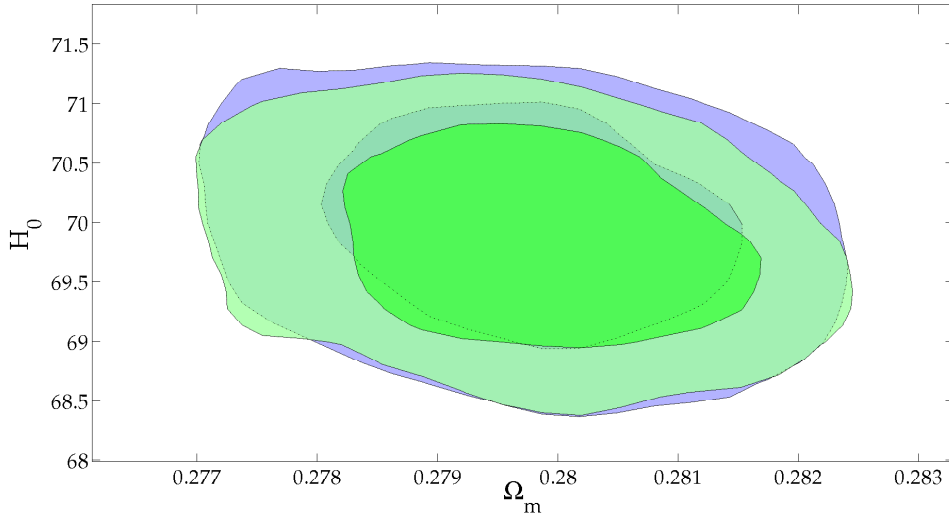


Figure 7.6: 1- and  $2\sigma$  confidence regions in the parameter space of  $\Omega_m$ ,  $H_0$ . The green figure represents case 1 (using only WL) and the blue figure case 3 (using WL + SNe Ia + RD). Both cases use a  $\Lambda$ CDM fiducial cosmology. The figures are almost identical, indicating that the constraining power on the parameters  $\Omega_m$  and  $H_0$  comes solely from weak lensing.

## 7.2 JBP fiducial cosmology

Two different probe configurations are used for the JBP fiducial cosmology: one with only SNe Ia and RD, and one including WL.

### 7.2.1 Case 4: supernovae Ia & redshift drift

Case 4 makes use of SN Ia and RD mock data, and the results are shown in fig. [7.7]. Since the  $w_0$  and  $w_a$  parameters of the CPL model are not physically equivalent to those of the JBP model, their fiducial values are not shown.

The characteristic shape of  $w_a$  present in case 2, which uses the same probe configuration, is also present in this case.

Since the JBP dark energy behaviour cannot be recovered by the CPL model, the cosmological parameters are expected to display a shift. The recovered mean values of  $\Omega_m$  and  $H_0$  are however within  $1\sigma$  of the fiducial values (with shifts of 0.1892 and 0.03816, respectively), thus the error is not significant with this probe configuration and its resulting parameter uncertainties.

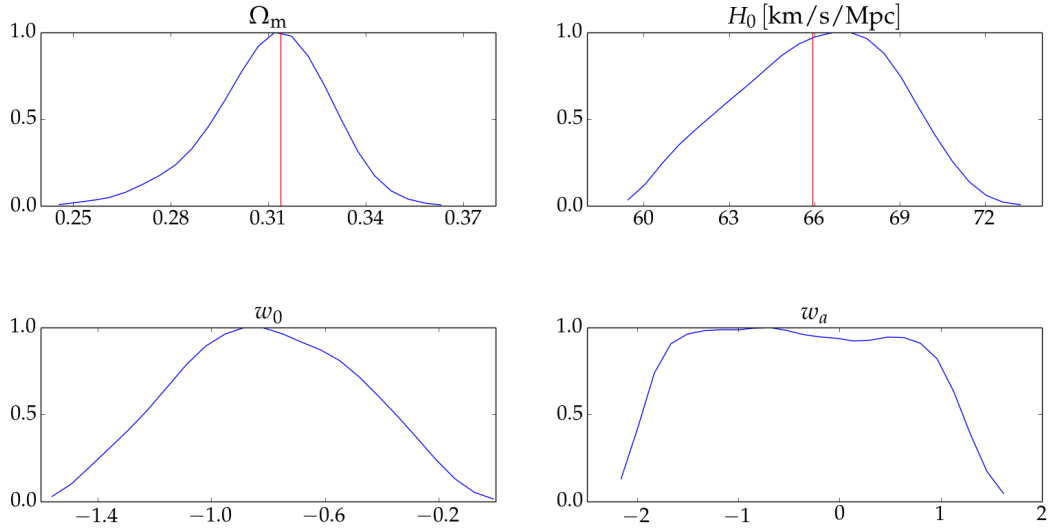


Figure 7.7: Marginalized posterior probability distributions of case 4: JBP fiducial cosmology, CPL framework cosmology, using SNe Ia and RD mock data. Red lines are fiducial values used to produce the mock data.

### 7.2.2 Case 5: weak lensing, supernovae Ia & redshift drift

Turning finally to the case of a JBP fiducial cosmology analyzed with all three probes, the marginalized posterior probability distributions are shown in fig. [7.8].

The  $\Omega_m$  ( $0.3115 \pm 0.001163$ ) and  $H_0$  ( $66.10 \pm 0.5605$ ) parameters have standard deviations 1.53 and 4.78 times smaller than in the previous case, respectively. This again emphasizes the constraining power of adding weak lensing as a probe.

While the mean value of  $H_0$  is within  $1\sigma$  of the fiducial value,  $\Omega_m$  is shifted by  $1.945\sigma$  and  $\sigma_8$  ( $0.7893 \pm 0.001336$ ) by  $1.511\sigma$ . The high sensitivity of the probe configuration thus leads to a bias on the cosmological parameter estimates.

The results suggest that, although the parameters may be determined to great precision by upcoming experiments such as Euclid, their values could be inaccurate if the assumed dark energy equation-of-state differs from the actual one. This demonstrates this work's hypothesized error on the cosmological parameters.

In order to overcome this error, a model-independent parametrization of  $w_{\text{DE}}$  could be used.

In this kind of approach, different data sets are sorted into redshift bins, and a likelihood analysis is performed for  $w(z)$  in each bin (Said et al., 2013). The sampled values are then interpolated between in a way that ensures a smooth and continuous  $w(z)$ . The method performs well, but has its limitations - since it is not possible to define the number of degrees of freedom in the likelihood analysis, the errors are difficult to estimate (Shafieloo, 2012).

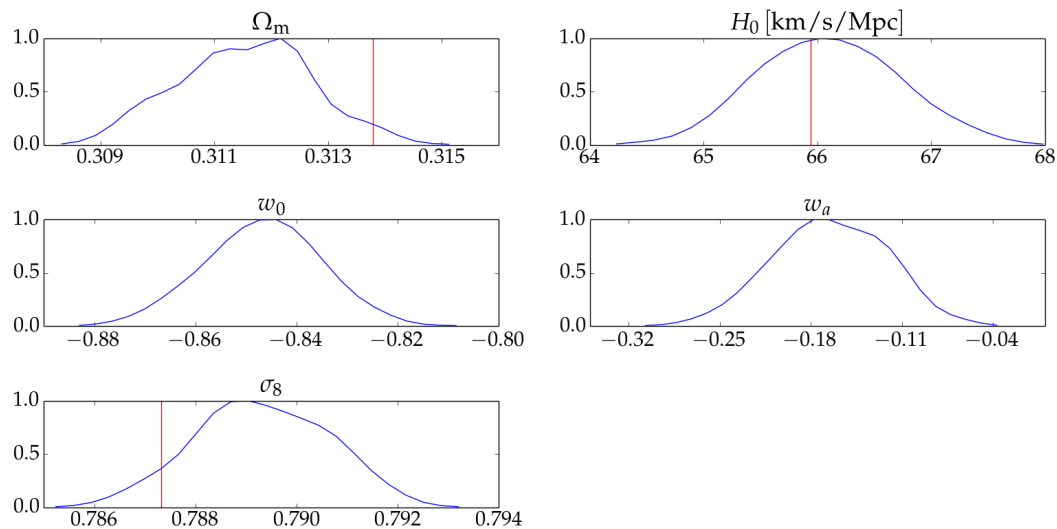


Figure 7.8: Marginalized posterior probability distributions for case 5: a JBP fiducial cosmology analyzed with a CPL framework cosmology. Red lines indicate fiducial values used to produce mock data of WL, SNe Ia and RD.

	Case 1	Shift	Case 2	Shift	Case 3	Shift
$\Omega_m$	$0.2797 \pm 1.123 \times 10^{-3}$	0.2492	$0.2762 \pm 0.01183$	0.3264	$0.2797 \pm 1.112 \times 10^{-3}$	0.2519
$H_0$	$69.84 \pm 0.5798$	0.06677	$70.79 \pm 1.745$	0.5673	$69.96 \pm 0.6168$	0.2497
$w_0$	$-1.002 \pm 0.01193$	0.1756	$-1.001 \pm 0.2615$	$3.507 \times 10^{-3}$	$-1.002 \pm 0.01160$	0.1887
$w_a$	$3.327 \times 10^{-3} \pm 0.04625$	0.07193	$-0.2703 \pm 0.9834$	0.2748	$2.911 \times 10^{-3} \pm 0.04525$	0.06434
$\sigma_8$	$0.8245 \pm 1.400 \times 10^{-3}$	0.1673	-	-	$0.8245 \pm 1.434 \times 10^{-3}$	0.1775

Table 7.3: Recovered mean values with standard deviations and shifts for cases 1, 2 and 3 using a  $\Lambda$ CDM fiducial cosmology. Case 1 uses weak lensing, case 2 supernovae Ia and redshift drift, and case 3 all three probes.

	Case 4	Shift	Case 5	Shift
$\Omega_m$	$0.3104 \pm 0.0178$	0.1892	$0.3115 \pm 1.163 \times 10^{-3}$	1.945
$H_0$	$66.04 \pm 2.678$	0.03816	$66.10 \pm 0.5605$	0.2596
$w_0$	$-0.8035 \pm 0.3080$	-	$-0.8467 \pm 0.01126$	-
$w_a$	$-0.3743 \pm 0.9307$	-	$-0.1653 \pm 0.04293$	-
$\sigma_8$	-	-	$0.7893 \pm 1.336 \times 10^{-3}$	1.511

Table 7.4: Recovered mean values with standard deviations and shifts for the two cases with a JBP fiducial cosmology. Case 4 uses only SN Ia and RD, while case 5 uses all three probes. The shifts of  $w_0$  and  $w_a$  are not calculated, since these parameters are not directly comparable to those of the fiducial model.

## 8 Conclusion

The aim of this work has been to quantify the error made on the cosmological parameters when assuming an incorrect form of the dark energy equation-of-state. Weak lensing, supernovae Ia and redshift drift mock data were produced in accordance with the upcoming Euclid (Euclid Science Study Team, 2011) and CODEX (Bonifacio et al. [CODEX], 2010) experiments for both a cosmological constant  $w_{\text{DE}} = -1$  and a JBP dark energy model with  $w_{\text{DE}}(z) = w_0 + w_a(a - a^2)$ . The mock data were fitted to theoretical equations derived from a cosmology including the CPL dark energy model ( $w_{\text{DE}}(z) = w_0 + w_a(1 - a)$ ) using a Monte Carlo Markov Chains method, and the recovered values of the cosmological parameters were compared to the input values of the mock data.

The parameter values used to create the cosmological constant mock data were recovered well with the CPL model. None of the recovered parameter mean values were found to be more than  $1\sigma$  away from the mock data values, regardless of whether the probes used were weak lensing, supernovae Ia and redshift drift, or all three combined.

This was not true for the analyses using a JBP model to produce the mock data. While no significant effect was found when using supernovae Ia and redshift drift, adding weak lensing as a probe caused a shift from the mock data values. The recovered mean values of the parameters  $\Omega_m$  and  $\sigma_8$  were then shifted by  $1.945\sigma$  and  $1.511\sigma$ , respectively.

This demonstrates that since the widely used CPL dark energy model cannot reproduce the features of the slightly different JBP dark energy model, the recovered cosmological parameter values can be shifted beyond one standard deviation. As future experiments increase their sensitivity, it is therefore crucial to avoid too simple parametrizations.

To expand on this work more general parametrizations could be tested to investigate their flexibility in recovering parameter values. Furthermore, it would be interesting to allow for non-zero neutrino masses, as this could possibly lead to reduced shifts, but a false detection of massive neutrinos.

## References

- R. Adam, P. A. R. Ade, N. Aghanim, et al. Planck intermediate results. XXX. The angular power spectrum of polarized dust emission at intermediate and high Galactic latitudes. *ArXiv e-prints*, Sept. 2014.
- P. A. R. Ade, N. Aghanim, C. Armitage-Caplan, et al. Planck 2013 results. XVI. Cosmological parameters. *Astronomy & Astrophysics*, 571:A16, Nov. 2014a. doi: 10.1051/0004-6361/201321591.
- P. A. R. Ade, R. W. Aikin, D. Barkats, et al. Detection of B-Mode Polarization at Degree Angular Scales by BICEP2. *Physical Review Letters*, 112(24):241101, June 2014b. doi: 10.1103/PhysRevLett.112.241101.
- M. Bartelmann and P. Schneider. Weak gravitational lensing. *Physics Reports*, 340:291–472, Jan. 2001. doi: 10.1016/S0370-1573(00)00082-X.
- T. Bayes and R. Price. An Essay towards Solving a Problem in the Doctrine of Chances. By the Late Rev. Mr. Bayes, F. R. S. Communicated by Mr. Price, in a Letter to John Canton, A. M. F. R. S. *Philosophical Transactions*, 53:370–418, 1763. doi: 10.1098/rstl.1763.0053. URL <http://rstl.royalsocietypublishing.org/content/53/370.short>.
- F. Bernardeau, C. Pitrou, and J.-P. Uzan. CMB spectra and bispectra calculations: making the flat-sky approximation rigorous. *Journal of Cosmology and Astroparticle Physics*, 2:015, Feb. 2011. doi: 10.1088/1475-7516/2011/02/015.
- P. Bonifacio, S. Cristiani, M. Dessauges, et al. E-ELT PROGRAMME. CODEX Phase A Study. The Science Case (Version 7.0). E-TRE-IOA-573-0001 Issue 1. <http://www.iac.es/proyecto/codex/pages/documents.php>, Jan. 2010.
- V. F. Cardone, S. Spiro, I. Hook, and R. Scaramella. Testing the distance duality relation with present and future data. *Physical Review D*, 85(12):123510, June 2012. doi: 10.1103/PhysRevD.85.123510.
- S. M. Carroll. *Spacetime and geometry. An introduction to general relativity*. Addison Wesley, 2004.
- M. Chevallier and D. Polarski. Accelerating Universes with Scaling Dark Matter. *International Journal of Modern Physics D*, 10:213–223, 2001. doi: 10.1142/S0218271801000822.
- S. Dodelson. *Modern cosmology*. Academic Press, 2003.
- A. Einstein. Die Feldgleichungen der Gravitation. *Sitzungsberichte der Königlich Preußischen Akademie der Wissenschaften*, pages 844–847, 1915.

- A. Einstein. Kosmologische Betrachtungen zur allgemeinen Relativitätstheorie. *Sitzungsberichte der Königlich Preußischen Akademie der Wissenschaften*, pages 142–152, 1917.
- D. J. Eisenstein and W. Hu. Baryonic Features in the Matter Transfer Function. *The Astrophysical Journal*, 496:605–614, Mar. 1998. doi: 10.1086/305424.
- D. J. Eisenstein, W. Hu, and M. Tegmark. Cosmic Complementarity:  $H_0$  and  $\Omega_m$  from Combining Cosmic Microwave Background Experiments and Redshift Surveys. *The Astrophysical Journal*, 504:L57–L60, Sept. 1998. doi: 10.1086/311582.
- Euclid Science Study Team. Euclid Assessment Study Report for the ESA Cosmic Visions. *ArXiv e-prints*, Dec. 2009.
- D. J. Fixsen. The Temperature of the Cosmic Microwave Background. *The Astrophysical Journal*, 707:916–920, Dec. 2009. doi: 10.1088/0004-637X/707/2/916.
- A. Friedmann. Über die Krümmung des Raumes. *Zeitschrift für Physik*, 10:377–386, 1922. doi: 10.1007/BF01332580.
- J. A. Frieman, M. S. Turner, and D. Huterer. Dark Energy and the Accelerating Universe. *Annual Review of Astronomy and Astrophysics*, 46:385–432, Sept. 2008. doi: 10.1146/annurev.astro.46.060407.145243.
- A. Gelman and D. B. Rubin. Inference from Iterative Simulation Using Multiple Sequences. *Statistical Science*, 7(4):457–472, 1992.
- G. Hinshaw, D. Larson, E. Komatsu, et al. Nine-year Wilkinson Microwave Anisotropy Probe (WMAP) Observations: Cosmological Parameter Results. *The Astrophysical Journal Supplement*, 208:19, Oct. 2013. doi: 10.1088/0067-0049/208/2/19.
- M. P. Hobson, A. H. Jaffe, A. R. Liddle, P. Mukherjee, and D. Parkinson. *Bayesian Methods in Cosmology*. Cambridge University Press, 2010.
- Y. Hu, M. Li, X.-D. Li, and Z. Zhang. Investigating the Possibility of a Turning Point in the Dark Energy Equation of State. *Science China Physics, Mechanics, and Astronomy*, 57:1607–1612, Aug. 2014. doi: 10.1007/s11433-014-5497-y.
- E. Hubble. A Relation between Distance and Radial Velocity among Extra-Galactic Nebulae. *Proceedings of the National Academy of Science*, 15:168–173, Mar. 1929. doi: 10.1073/pnas.15.3.168.
- D. Huterer. Weak lensing, dark matter and dark energy. *General Relativity and Gravitation*, 42: 2177–2195, Sept. 2010. doi: 10.1007/s10714-010-1051-z.

- H. K. Jassal, J. S. Bagla, and T. Padmanabhan. WMAP constraints on low redshift evolution of dark energy. *Monthly Notices of the Royal Astronomical Society*, 356:L11–L16, 2005. doi: 10.1111/j.1745-3933.2005.08577.x.
- O. Lahav and A. R. Liddle. The Cosmological Parameters 2014. *ArXiv e-prints*, Jan. 2014.
- G. Lemaître. L'Univers en expansion. *Annales de la Societe Scietifique de Bruxelles*, 53:51, 1933.
- A. Lewis. CosmoMC, cosmological MonteCarlo. <http://cosmologist.info/cosmomc/>, 2012. October 2012 version.
- A. Lewis and S. Bridle. Cosmological parameters from CMB and other data: A Monte Carlo approach. *Physical Review D*, 66(10):103511, Nov. 2002. doi: 10.1103/PhysRevD.66.103511.
- E. Linder. Exploring the expansion history of the universe. *Physical Review Letters*, 90(9):091301, Mar. 2003. doi: 10.1103/PhysRevLett.90.091301.
- A. Loeb. Direct Measurement of Cosmological Parameters from the Cosmic Deceleration of Extragalactic Objects. *The Astrophysical Journal Letters*, 499:L111–L114, June 1998. doi: 10.1086/311375.
- M. Martinelli, S. Pandolfi, C. J. A. P. Martins, and P. E. Vielzeuf. Probing dark energy with redshift drift. *Physical Review D*, 86(12):123001, Dec. 2012. doi: 10.1103/PhysRevD.86.123001.
- P. J. E. Peebles. *Principles of Physical Cosmology*. Princeton University Press, 1993.
- S. Perlmutter, G. Aldering, G. Goldhaber, et al. Measurements of  $\Omega$  and  $\Lambda$  from 42 High-Redshift Supernovae. *The Astrophysical Journal*, 517:565–586, June 1999. doi: 10.1086/307221.
- A. G. Riess, A. V. Filippenko, P. Challis, et al. Observational Evidence from Supernovae for an Accelerating Universe and a Cosmological Constant. *The Astrophysical Journal*, 116:1009–1038, Sept. 1998. doi: 10.1086/300499.
- H. P. Robertson. Kinematics and World-Structure. *The Astrophysical Journal*, 82:284, Nov. 1935. doi: 10.1086/143681.
- S. Rosswog and M. Brüggen. *Introduction to High-Energy Astrophysics*. Cambridge University Press, Aug. 2007.
- B. Ryden. *Introduction to cosmology*. Addison Wesley, 2003.
- N. Said, C. Baccigalupi, M. Martinelli, A. Melchiorri, and A. Silvestri. New constraints on the dark energy equation of state. *Physical Review D*, 88(4):043515, Aug. 2013. doi: 10.1103/PhysRevD.88.043515.

- A. Sandage. The Change of Redshift and Apparent Luminosity of Galaxies due to the Deceleration of Selected Expanding Universes. *The Astrophysical Journal*, 136:319, Sept. 1962. doi: 10.1086/147385.
- M. I. Scrimgeour, T. Davis, C. Blake, et al. The WiggleZ Dark Energy Survey: the transition to large-scale cosmic homogeneity. *Monthly Notices of the Royal Astronomical Society*, 425: 116–134, Sept. 2012. doi: 10.1111/j.1365-2966.2012.21402.x.
- A. Shafieloo. Crossing statistic: reconstructing the expansion history of the universe. *Journal of Cosmology and Astroparticle Physics*, 8:002, Aug. 2012. doi: 10.1088/1475-7516/2012/08/002.
- A. G. Walker. On the formal comparison of Milne's kinematical system with the systems of general relativity. *Monthly Notices of the Royal Astronomical Society*, 95:263–269, Jan. 1935.
- S. Weinberg. Anthropic bound on the cosmological constant. *Physical Review Letters*, 59:2607–2610, Nov 1987. doi: 10.1103/PhysRevLett.59.2607.
- F. Zwicky. Die Rotverschiebung von extragalaktischen Nebeln. *Helvetica Physica Acta*, 6:110–127, 1933.

## A Appendix

	Case 1	Shift	Case 2	Shift	Case 3	Shift
$\Omega_b h^2$	$0.02264 \pm 5.649 \times 10^{-4}$	$2.532 \times 10^{-3}$	$0.02267 \pm 5.739 \times 10^{-4}$	0.05213	$0.02276 \pm 8.282 \times 10^{-4}$	0.1392
$\Omega_{\text{DM}} h^2$	$0.1138 \pm 1.791 \times 10^{-3}$	0.01145	$0.1156 \pm 4.793 \times 10^{-3}$	0.3767	$0.1142 \pm 1.679 \times 10^{-3}$	0.2132
$\theta$	$1.039 \pm 2.950 \times 10^{-3}$	$3.390 \times 10^{-3}$	$1.040 \pm 6.411 \times 10^{-3}$	0.07019	$1.040 \pm 2.432 \times 10^{-3}$	0.1645
$\tau$	$0.07890 \pm 0.02874$	0.3515	$0.07913 \pm 0.02877$	0.3431	$0.08139 \pm 0.02866$	0.2656
$n_S$	$0.9719 \pm 2.477 \times 10^{-3}$	0.04986	$1.005 \pm 0.2902$	0.1131	$0.9714 \pm 2.144 \times 10^{-3}$	0.2619
$\log(10^{10} A_S)$	$3.180 \pm 0.01138$	0.02275	$3.367 \pm 0.3717$	0.5042	$3.179 \pm 0.01050$	0.08222
$\Omega_m$	$0.2797 \pm 1.123 \times 10^{-3}$	0.2492	$0.2762 \pm 0.01183$	0.3264	$0.2797 \pm 1.112 \times 10^{-3}$	0.2519
$H_0$	$69.84 \pm 0.5798$	0.06677	$70.79 \pm 1.745$	0.5673	$69.96 \pm 0.6168$	0.2497
$w_0$	$-1.002 \pm 0.01193$	0.1756	$-1.001 \pm 0.2615$	$3.507 \times 10^{-3}$	$-1.002 \pm 0.01160$	0.1887
$w_a$	$3.327 \times 10^{-3} \pm 0.04625$	0.07193	$-0.2703 \pm 0.9834$	0.2748	$2.911 \times 10^{-3} \pm 0.04525$	0.06434
$\sigma_8$	$0.8245 \pm 1.400 \times 10^{-3}$	0.1673	-	-	$0.8245 \pm 1.434 \times 10^{-3}$	0.1775

Table A.1: Recovered mean values with standard deviations and shifts for cases 1, 2 and 3 using a  $\Lambda$ CDM fiducial cosmology. Case 1 uses weak lensing, case 2 supernovae Ia and redshift drift, and case 3 all three probes.

	Case 4	Shift	Case 5	Shift
$\Omega_b h^2$	$0.02228 \pm 1.305 \times 10^{-3}$	0.2783	$0.02238 \pm 8.651 \times 10^{-4}$	0.2989
$\Omega_{\text{DM}} h^2$	$0.1131 \pm 0.01041$	0.06980	$0.1137 \pm 1.767 \times 10^{-3}$	0.03152
$\theta$	$1.041 \pm 9.052 \times 10^{-3}$	0.2433	$1.039 \pm 2.551 \times 10^{-3}$	0.07094
$\tau$	$0.08006 \pm 0.02884$	0.3102	$0.07997 \pm 0.02965$	0.3045
$n_S$	$0.9851 \pm 0.2899$	0.04509	$0.9707 \pm 2.205 \times 10^{-3}$	0.5943
$\log(10^{10} A_S)$	$3.345 \pm 0.3784$	0.4368	$3.177 \times 0.01036$	0.2669
$\Omega_m$	$0.3104 \pm 0.0178$	0.1892	$0.3115 \pm 1.156 \times 10^{-3}$	1.945
$H_0$	$66.04 \pm 2.678$	0.03816	$66.10 \pm 0.6138$	0.2596
$w_0$	$-0.8035 \pm 0.3080$	-	$-0.8467 \pm 0.01139$	-
$w_a$	$-0.3743 \pm 0.9307$	-	$-0.1653 \pm 0.04332$	-
$\sigma_8$	-	-	$0.7893 \pm 1.317 \times 10^{-3}$	1.511

Table A.2: Recovered mean values with standard deviations and shifts for the two cases with a JBP fiducial cosmology. Case 4 uses only SN Ia and RD, while case 5 uses all three probes. The shifts of  $w_0$  and  $w_a$  are not calculated, since these parameters are not directly comparable to those of the fiducial model.